

ImputeFormer: Low Rankness-Induced Transformers for Generalizable Spatiotemporal Imputation

Tong Nie, *Student Member, IEEE*, Guoyang Qin, Wei Ma, *Member, IEEE*, Yuewen Mei, and Jian Sun*

Abstract—Missing data is a pervasive issue in both scientific and engineering tasks, especially for the modeling of spatiotemporal data. This problem attracts many studies to contribute to machine learning solutions. Existing imputation solutions mainly include low-rank models and deep learning models. On the one hand, low-rank models assume general structural priors, but have limited model capacity. On the other hand, deep learning models possess salient features of expressivity while lacking prior knowledge of the underlying spatiotemporal process. Leveraging the strengths of both two paradigms, we demonstrate a low rankness-induced Transformer model to achieve a balance between strong inductive bias and high model expressivity. The exploitation of the inherent structures of spatiotemporal data enables our model to learn balanced signal-noise representations, making it versatile for a variety of imputation problems. We demonstrate its superiority in terms of accuracy, efficiency, and generality in heterogeneous datasets, including traffic speed, traffic volume, solar energy, smart meters, and air quality. Comprehensive case studies are performed to further strengthen interpretability. Promising empirical results provide strong conviction that incorporating time series primitives, such as low-rank properties, can substantially facilitate the development of a generalizable model to approach a wide range of spatiotemporal imputation problems. The model implementations will be open source at: <https://github.com/tongnie/ImputeFormer>.

Index Terms—Transformers, Data Imputation, Low-Rank Modeling, Spatiotemporal Data, Time Series, Graph Neural Networks.



1 INTRODUCTION

MISSING data is a common challenge in detection systems, especially in high-resolution monitoring systems. Factors such as inclement weather, energy supply, sensor service time, and lighting conditions can adversely affect the quality of monitoring data [1], [2], [3]. Given these factors, the data missing rates can be quite high. For example, the air quality monitoring data in the Urban Air project [4] contain approximately 30% of the measurements being invalid or missing due to station malfunction. Similarly, subsets of Uber Movement data, such as the New York City dataset, have an approximate 85% of records missing [5].

This problem encourages researchers to develop advanced models that can combine the available information from limited observations to fill in any missing values. Extensive research has contributed to machine learning methods for this purpose, especially in the field of spatiotemporal data [1], [2], [3], [6], [7], [8], [9], [10], [11]. Generally, there are two research paradigms for imputing missing data. The first paradigm uses low-rank and low-dimensional analytical models, such as [6], [9], [11], [12], [13], which assumes the data has a well-structured matrix or tensor form. These models utilize the algebraic properties of the assumed structure, such as low-rankness, low nuclear

norm, and spectrum sparsity (we use the term “low-rank” as a proxy), to impute missing values [14]. While simple low-rank models like matrix factorization and tensor completion can effectively handle incomplete data, they may struggle with capturing complex patterns, such as nonlinearity and nonstationarity. When learning low-rank representations, these models can excessively smooth the reconstructed data, filtering out informative signals, and generating an over-squashing reconstruction in some cases [15].

The second paradigm uses deep learning-based imputation models. These models learn the dynamics of the data-generating process and demonstrate improved performance [16], [17], [18], [19], [20], [21]. However, despite the success of deep neural imputation models on various benchmarks, there are still costs and difficulties that need further attention. First, such data-intensive methods require a substantial amount of training expenses due to the complex model structures in deep learning, such as probabilistic diffusion and bidirectional recurrence. This can consume significant computational memory and resources, making them less efficient for real-time deployment. Second, empirical loss-based learning methods, without the guidance of physics or data structures, are prone to overfitting and perform poorly when applied to tasks that fall outside the distribution.

The field of deep learning imputation has recently seen a shift from RNNs and diffusion to Transformer [19], [20], [22]. Transformer-based architecture is particularly notable for its efficient generative output and high expressivity, allowing more effective imputations compared to autoregression-based models. Although Transformers have the potential to serve as foundational architectures for general time series forecasting problems [23], [24], directly applying them to the

- Tong Nie, Guoyang Qin, Yuewen Mei, and Jian Sun are with the Department of Traffic Engineering, Tongji University, Shanghai, China (E-mail: {nietong, 2015qgy, meiyuewen, sunjian}@tongji.edu.cn).
- Wei Ma is with the Department of Civil and Environmental Engineering, The Hong Kong Polytechnic University, Hong Kong, SAR, China (E-mail: wei.w.ma@polyu.edu.hk).
- Corresponding author: Jian Sun.

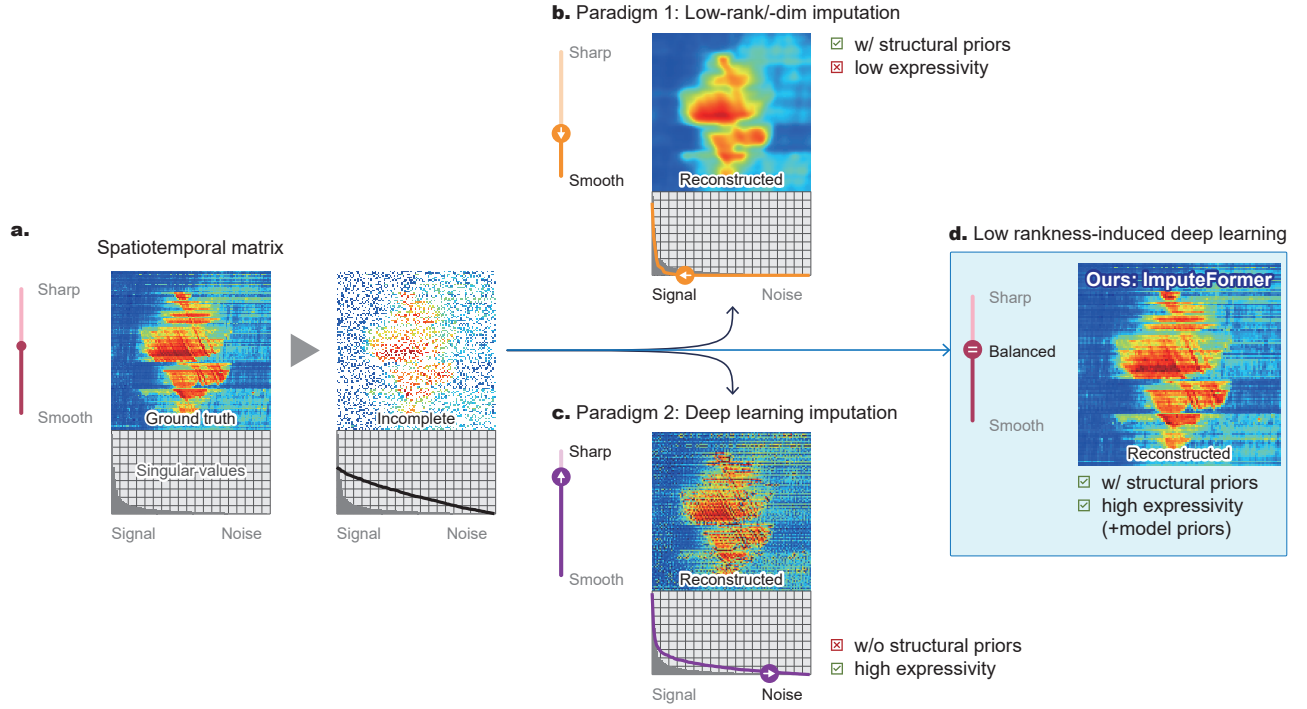


Fig. 1: Our motivation: (a) Spatiotemporal data generally exhibit a long-tailed distribution of singular value. The existence of missing data can significantly increase the rank (or singular values) of spatiotemporal matrix. (b) Low-rank models such as matrix factorization can filter out informative signals and generate a smooth reconstruction. The resulting spectrum truncates too much energy in its left part. (c) Deep learning models can preserve high-frequency noise and generate sharp imputation. The singular spectrum maintains too much energy for the right part. With the generality of low-rank models and the expressivity of deep models, ImputeFormer model achieves a signal-noise balance for accurate imputation.

imputation task can be problematic. Modern deep learning techniques, such as self-attention and residual connections, can mistakenly preserve high-frequency noise in data as informative signals [25]. This can lead the model to learn high-rank representations that hinder accurate imputation. Moreover, the existence of missing data can introduce spurious correlations between “tokens”, posing challenges to this architecture. Given the above concerns, imposing a low-rank inductive bias on the Transformer structure appears to offer an opportunity to enhance both the effectiveness and efficiency in the context of spatiotemporal imputation.

In summary, matrix- and tensor-based models provide useful priors for spatiotemporal data, such as low-rankness and sparsity. However, their ability to represent data is limited (see Fig. 1(b)). On the other hand, deep learning models, especially the Transformers, excel at learning representations, but lack prior knowledge of data generation (see Fig. 1(c)). With the increasing demand for a versatile and adaptable model that can handle various imputation problems in the real world, such as cross-domain datasets, different observation conditions, highly sparse measurements, and different input patterns, existing advanced solutions that were typically evaluated on limited datasets with simple settings may not be generalizable. For example, they may use traffic speed data with a fixed missing pattern for evaluation, leaving it questionable whether these solutions are effective in handling various other data types and more challenging scenarios. Therefore, there is a temptation to combine these two paradigms and leverage their strengths

to explore an alternative paradigm that can address general imputation scenarios for spatiotemporal data.

In this paper, we exploit the structural priors of low-rankness to power the canonical Transformer model (see Fig. 1(d)) to achieve state-of-the-art imputation performance on various spatiotemporal benchmarks. Specifically, we propose a projected attention mechanism on the temporal dimension and a global adaptive graph convolution on the spatial dimension to equivalently achieve the attention factorization and introduce low-rankness. A Fourier sparsity loss is further developed to regularize the spectrum of solution. For brevity, we term our model *Spatiotemporal Imputation Transformers* (ImputeFormer). ImputeFormer can achieve a good signal-noise balance by inheriting the merits of low-rank and deep learning models. Our main methodological and technical contributions include:

- 1) We power the Transformers with low-rankness inductive bias to achieve a balance between signal and noise for general spatiotemporal data imputation.
- 2) We showcase its superiority in terms of accuracy, efficiency, and generality in heterogeneous datasets, including traffic, solar, electricity, and air quality.
- 3) Comprehensive case studies and comparison with state-of-the-art benchmark methods reveal the versatility and interpretability of ImputeFormer.

The rest of this article is organized as follows. Section 2 reviews related work and specifies the notation. Section 3 details the architectural and modular designs. In Section 4,

we evaluate our model on various benchmarks and comprehensive discussions are provided. Section 5 concludes this work and provides potential directions.

2 PRELIMINARY AND RELATED WORK

2.1 Notations and Problem Formulations

Key Notations: This section first introduces some notation following the terminology used in previous work [20]. In a sensor network with N static detectors at some measurement positions, spatiotemporal data with context information can be obtained: (1) $\mathbf{X}_{t:t+T} \in \mathbb{R}^{N \times T}$: The observed (incomplete) data matrix containing missing values collected by all sensors over a time interval $\mathcal{T} = \{t, \dots, t+T\}$, where T represents the observation period; (2) $\mathbf{Y}_{t:t+T} \in \mathbb{R}^{N \times T}$: the ground truth (complete) data matrix used for evaluation; (3) $\mathbf{U}_{t:t+T} \in \mathbb{R}^{T \times d_u}$: Exogenous variables describe time series, such as the time of day, day of week, and week of month information; (4) $\mathbf{V} \in \mathbb{R}^{N \times d_v}$: Sensor-specific meta-information, such as detector ID and location of installation. For ease of representation, this paper uses the terms node, sensor, and location interchangeably.

Problem Formulation: Given the above elements, the multivariate time series imputation problem can be defined as an inductive learning and inference process:

$$\text{Learning } \hat{\Theta} = \arg \min_{\Theta} \sum_{t \in \mathcal{T}} \ell(\text{NN}(\{\mathbf{x}_t, \mathbf{u}_t, \mathbf{m}_t\}, \mathbf{V}|\Theta), \mathbf{x}_t),$$

$$\text{Inference } \hat{\mathbf{x}}_{t'} = \text{NN}(\{\mathbf{x}_{t'}, \mathbf{u}_{t'}, \mathbf{m}_{t'}\}, \mathbf{V}|\hat{\Theta}), \forall \{t' \dots t' + T\}, \quad (1)$$

where $\text{NN}(\cdot|\Theta)$ is the neural network model parameterized by Θ , and the indicator \mathbf{m}_t denotes the locations of the masked values for training and the locations of the observed values for inference. After training the model on observed data, the imputation model can act on a different time scale from the training set. It is worth mentioning that the ground truth \mathbf{Y} is only used to calculate the evaluation metrics and is not available to the model in this process.

2.2 Related Works

This section provides a review of the literature on the multivariate time series imputation problem. Generally, there exist two series of studies on this topic, including 1) low-dimensional/rank models and 2) deep imputation models. Besides, we also discuss existing Transformer-based imputation solutions and techniques for time series self-supervised learning to clarify the connections between our models.

Low-Dimensional and Low-Rank Imputation Models:

Early methods approached the series data imputation problem by exploring statistical interpolation tools [26], [27]. Recently, low-rank matrix factorization (MF) [13], [28] and low-rank tensor completion models (LRTC) [6], [9], [10], [12], [29] have emerged as numerically efficient techniques for spatiotemporal imputation. To incorporate series-related inductive biases, TRMF [28] imposed autoregressive regularization on the temporal manifold. TIDER [13] decomposed the temporal component into trend, seasonality and bias representations under the MF framework. Despite being conceptually intuitive and concise, the strong assumption about data structure and limited model capacity hinder the real-world efficacy of these low-dimensional models.

Deep Learning Imputation Models: Recent advancements in neural time series analysis open a new horizon to improve imputation performance. Unlike time series forecasting models, most deep imputation methods learn to reconstruct the distribution of observed data or aggregate pointwise information progressively [30]. Representative methods include GRU-D [17], GRUI [31], BRITS [16], GAIN [32], E2GAN [33] NAOMI [34], CSDI [35], PrISTI [21] NRTSI [36]. To harness the multivariate nature of spatiotemporal data, graph neural networks (GNNs) have been adopted to model sensor-wise correlations for more complicated missing patterns. In particular, MDGCN [37] and GACN [8] applied GNNs with RNNs for traffic data imputation. IGNNK [38], STAR [39], and STCAGCN [40] further tackle the kriging problem, which is a special data imputation scenario. As a state-of-the-art model and an architectural template for GNN-RNN models, GRIN [18] is based on a message passing GRU architecture that progressively performed a two-stage forward and backward recurrent message aggregation. GNNs are employed to encode predefined relational biases.

Transformers for Time Series Imputation: Transformers [41] can aggregate abundant information from arbitrary elements within the input, becoming a natural choice for the missing sequential data imputation. In particular, CDSA [22] developed a cross-channel self-attention that can utilize correlations in different dimensions. SAITS [19] combined the masked imputation task with an observed reconstruction task, and applied a diagonally-masked self-attention to hierarchically reconstruct the input data. SPIN [20] achieved state-of-the-art imputation performance by conducting a sparse cross-attention and a temporal self-attention on all observed spatiotemporal points. A two-phase data propagation and a hierarchical loss are also adopted to improve the performance. However, self-attention in the spatial dimension with $\mathcal{O}(N^2)$ (N is the node number) complexity hinders its application in larger graphs.

Time Series Masked Modeling: As the data imputation task is basically conditioned on the reconstruction of artificially masked time points or subseries, it seamlessly connects with the time series representation learning problem. Masked time series modeling (MTM) focuses mainly on learning hidden representations for time series by using self-supervised training techniques [42], [43], [44]. Ti-MAE [44] proposed reconstructing the randomly masked series embedding using a Transformer encoder. PatchTST [43] handled masked patches in long-term series. SimMTM [42] aggregates point-wise information by series-wise similarities. The main difference between time series imputation and representation learning lies in the way missing (masked) values are injected and the training objective. The canonical MTM aims to learn the neural representation that benefits the downstream task, and the masking can be performed regularly for each series during the training stage. In contrast, series imputation tackles missing values that occurred before training, and the model is optimized to reduce the reconstruction error as much as possible by resorting to the MTM on the observed part of the series.

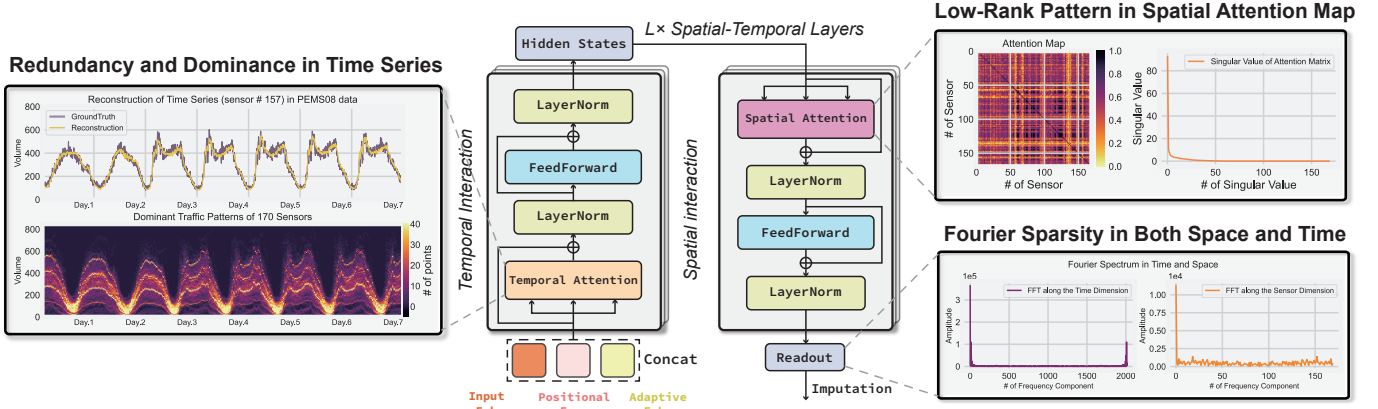


Fig. 2: Illustration on the low-rankness nature in time series and the induced ImputeFormer architecture. (a) Redundancy in time series: there are five dominant traffic patterns in the PEMS08 data that correspond to the five largest singular values, and a reasonable reconstruction of traffic volume can be achieved using only these five singular values. (b) Low-rank pattern in spatial attention map: the singular values of the multivariate correlation (attention) map show a long-tailed distribution and most of them are small values. (c) Fourier sparsity in both space and time dimensions: Spectral analysis reveals that both the spatial and temporal signals possess a sparse Fourier spectrum, with most amplitudes close to zero.

3 LOW RANKNESS-INDUCED TRANSFORMERS AS GENERALIZABLE SPATIOTEMPORAL IMPUTERS

This section elaborates the proposed ImputeFormer model. We first provide an architectural overview of the structure in Section 3.1 and then detail the input embedding design in Sections 3.2 and the spatial-temporal block in Sections 3.3 and 3.4. We provide an illustration to demonstrate the structural difference between different architectures in Fig. 3. The major difference between our model and the canonical Transformer is the integration of low-rank factorization. Unlike graph convolutional networks (GCNs), ImputeFormer does not require a predefined graph due to the global adaptive interaction between the series. It also bypasses the use of intricate techniques adopted in recent work such as bidirectional recurrent aggregation, sparse cross-attention, attention masking, and hierarchical loss functions. In addition, our model achieves linear complexity with respect to spatial and temporal dimensions.

3.1 Architectural Overview

The overall structure of the proposed ImputeFormer model is shown in Fig. 2. The input embedding layer transforms sparse observations to hidden states in an additional dimension and incorporates both fixed and learnable embedding into the inputs. Following a Time-and-Graph template [45], TemporalInteraction and SpatialInteraction perform global message passing alternatively on all spatiotemporal coordinates, producing imputed representations of missing points. Finally, a MLP readout is adopted to output the final imputation. The above process can be summarized as follows.

$$\begin{aligned}
 \mathcal{Z}_{t:t+T}^{(0)} &= \text{InputEmb}(\mathbf{X}_{t:t+T}, \mathbf{U}_{t:t+T}, \mathbf{V}), \\
 \mathcal{Z}_{t:t+T}^{(\ell+1)} &= \text{TemporalInteraction}(\mathcal{Z}_{t:t+T}^{(\ell)}), \\
 \mathcal{Z}_{t:t+T}^{(\ell+1)} &= \text{SpatialInteraction}(\mathcal{Z}_{t:t+T}^{(\ell+1)}), \forall \ell \in \{0, \dots, L\}, \\
 \hat{\mathbf{X}}_{t:t+T} &= \text{Readout}(\mathcal{Z}_{t:t+T}^{(L+1)}).
 \end{aligned} \tag{2}$$

The canonical Transformer block [41] can be adopted in TemporalInteraction and SpatialInteraction to gather spatial-temporal information for imputation. However, we argue that directly applying self-attention to the imputation problem is questionable. On the one hand, the calculation of pairwise attention is prone to sensitivity toward input data. This results in spurious correlations on top of sparse data that could be misleading. On the other hand, time series are typically low-rank in nature [46]. Full-attention computation on raw data can be overcorrelated and generate high-rank attention maps and estimations. To address these issues, we start from time series primitives and enhance the Transformer using these structural priors.

3.2 Spatiotemporal Input Embedding

Input Embedding: Unlike images or languages, time series are supposed to have low semantic densities [42], [43]. To exploit this inductive bias, many series forecasting models propose flattening and abstracting the input series to reduce information redundancy [47], [48], [49]. Specifically, given the input multivariate series $\mathbf{X}_{t:t+T} \in \mathbb{R}^{N \times T}$, each series can be represented by a multilayer perceptron (MLP): $\mathbf{z}^{i,(0)} = \text{MLP}(\mathbf{x}^i)$, where $\text{MLP}(\cdot) : \mathbb{R}^T \rightarrow \mathbb{R}^D$ is shared between each series.

However, we claim that this technique can be problematic for series imputation. If we express this mapping as the following expansion:

$$x_{t+h} = \sigma \left(\sum_{k=0}^T w_{k,h} x_{t+k} + b_{k,h} \right), \quad h \in \{0, \dots, T\}, \tag{3}$$

it is evident that the linear weights only depends on the relative position in the sequence and are agnostic to the data flow. Since missing data points and intervals can occur at arbitrary locations in the series, fixed weights can learn spurious relationships between each time step, thus overfitting the missing patterns in the training data.

Therefore, we should avoid using linear mappings on the time axis to account for the varying missing time points.

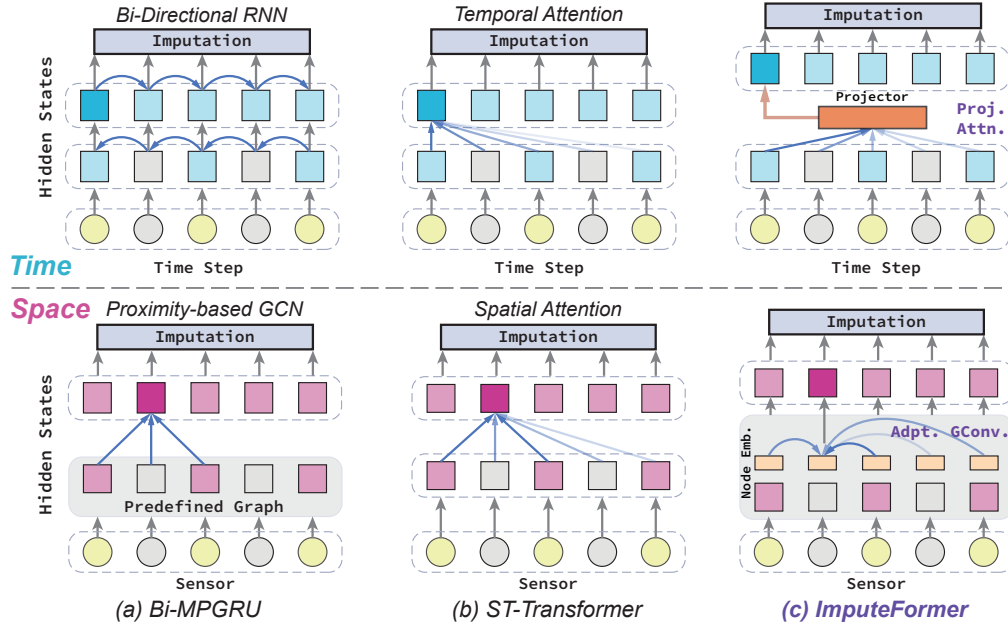


Fig. 3: Comparison of different imputation architectures. We illustrate how different methods approach the spatial and temporal message passing. (a) RNN-GCN model adopts bidirectional RNNs to gather available readings from consecutive time points and GCN to collect neighborhood information on predefined graphs. (b) Transformer model computes all pairwise correlations of the raw data on both spatial and temporal dimensions. (c) ImputeFormer utilizes projected attention along the temporal axis and global adaptive graph convolution based on node embedding in the spatial axis.

To this end, we adopt a dimension expansion strategy [50] to preserve the information density of the input series. In practice, we expand an additional dimension of the input incomplete series and project it into a hidden state along this new dimension:

$$\mathbf{Z}_{t:t+T}^{(0)} = \text{MLP}(\text{Unsqueeze}(\mathbf{X}_{t:t+T}, \text{dim}=-1), \quad (4)$$

where $\text{Unsqueeze}(\cdot) : \mathbb{R}^{N \times T} \rightarrow \mathbb{R}^{N \times T \times 1}$, and $\mathbf{Z}_{t:t+T}^{(0)} \in \mathbb{R}^{N \times T \times D}$ is the initial hidden representation. With this, we can aggregate message from other time points by learning data-dependent weights:

$$\mathbf{Z}_{t:t+T}^{i,(\ell+1)} = \mathcal{F}_\ell(\mathbf{Z}_{t:t+T}^{i,(\ell)})\mathbf{Z}_{t:t+T}^{i,(\ell)}, \quad (5)$$

where $\mathcal{F}_\ell(\cdot) : \mathbb{R}^{T \times D} \rightarrow \mathbb{R}^{T \times T}$ represents a data-driven function at the ℓ -th layer, such as self-attention.

Time Stamp Encoding: Time stamp encoding is adopted to handle the order-agnostic nature of Transformers [41]. As the input series covers a relatively short range, we only consider the time-of-day information. We adopt the sinusoidal positional encoding in [41] to inject the time-of-day information of each time series along time dimension:

$$\begin{aligned} p_{\text{sine}}^t &= \sin(p_t * 2\pi/\delta_D), \\ p_{\text{cosine}}^t &= \cos(p_t * 2\pi/\delta_D), \\ \mathbf{u}_t &= [p_{\text{sine}}^t \| p_{\text{cosine}}^t], \end{aligned} \quad (6)$$

where p_t is the index of t -th time-of-day point in the series, and δ_D is the day-unit time mapping. We concatenate \mathbf{p}_{sine} and $\mathbf{p}_{\text{cosine}}$ as the final time stamp encoding $\mathbf{U}_{t:t+T} \in \mathbb{R}^{T \times 2}$. Note that learnable series encoding is also optional.

Spatiotemporal Node Embedding: We consider the use of both predefined and learnable positional encodings as

input embeddings for the input series. Previous work has demonstrated the importance of node identification in distinguishing different sensors for spatiotemporal forecasting problems [47], [48], [51], [52]. Here we also recommend the use of learnable node embedding for imputation task. On the one hand, it benefits the adaptation of local components [51] in graph-based data structure. On the other hand, node embedding can be treated as a low-rank representation (an abstract and compact representation) of the incomplete series, which will be detailed in Section 3.4.

To implement, we can assign each series a random initialized parameter $\mathbf{e}^i \in \mathbb{R}^{D_s}$. We then split the hidden dimension of the static node embedding equally by the length of the time window (we assume that the variable dimension is an integer multiple of the length of the time window) as a *multi-head* node embedding and unfold it to form a low-dimensional and time-varying representation: $\mathbf{E}_{t:t+T}^i \in \mathbb{R}^{T \times D_s/T}$. The implicit interactions between the node embedding, data, and modular components are involved in the end-to-end gradient descent process. Finally, the spatiotemporal input embedding for each node can be formulated as follows:

$$\mathbf{Z}_{t:t+T}^{i,(1)} = \text{Concat}(\mathbf{Z}_{t:t+T}^{i,(0)}; \mathbf{U}_{t:t+T}; \mathbf{E}_{t:t+T}^i, \text{dim}=-1), \quad (7)$$

where $\mathbf{Z}_{t:t+T}^{i,(1)} \in \mathbb{R}^{T \times (D+D_s/T+2)}$ is input to the following modules. We will detail each modular design of the spatial-temporal block in the following sections.

3.3 Temporal Interaction with Projected Attention

Self-attention technique has been widely adopted to model temporal relations in both short- and long-term time series

forecasting studies [7], [43], [52], [53]. Given a hidden representation $\mathbf{Z}^{i,(\ell)} \in \mathbb{R}^{T \times D'}$ (subscripts are omitted for the sake of brevity), the canonical multi-head self-attention [41] is computed as follows:

$$\begin{aligned}\tilde{\mathbf{Z}}^{i,(\ell)} &= \text{LayerNorm}(\mathbf{Z}^{i,(\ell)} + \\ &\quad \text{SelfAtten}(\mathbf{Z}^{i,(\ell)}, \mathbf{Z}^{i,(\ell)}, \mathbf{Z}^{i,(\ell)})), \\ \mathbf{Z}^{i,(\ell+1)} &= \text{LayerNorm}(\tilde{\mathbf{Z}}^{i,(\ell)} + \\ &\quad \text{FeedForward}(\tilde{\mathbf{Z}}^{i,(\ell)})),\end{aligned}\quad (8)$$

where $\text{SelfAtten}(\mathbf{Z}, \mathbf{Z}, \mathbf{Z})$ transforms the input into queries $\mathbf{Q} \in \mathbb{R}^{T \times D'}$, keys $\mathbf{K} \in \mathbb{R}^{T \times D'}$, as well as values $\mathbf{V} \in \mathbb{R}^{T \times D'}$, and then outputs a weighted sum of the values according to attention scores as $\text{Softmax}(\mathbf{Q}\mathbf{K}^\top/\sqrt{D'})\mathbf{V}$.

Intuitively, the representations at unobserved locations can attend to all other observations and obtain a plausible new representation after a series of temporal attentive aggregations. However, after dimension expansion in Eq. (4), there exist varying degrees of redundancy in temporal information. The hidden dimension is practically much larger than the length of the sequence $D' \gg T$, then the attention score $\mathbb{R}^{T \times D'} \times \mathbb{R}^{D' \times T} \rightarrow \mathbb{R}^{T \times T}$ can be a high-rank matrix. In addition, simply collecting observations may incur a high computational cost for long sequences.

As is evident in Fig. 2, time series are supposed to be redundant in the time domain, that is, most of the information can be well reconstructed using only a few dominant modes. Imposing a low-rank constraint on the attentive process of incomplete series can facilitate the reconstruction of hidden spaces. Inspired by the efficient Transformer techniques in [54], we propose a projected attention mechanism with linear complexity to efficiently model the pairwise temporal interactions between all available time points in a lower-dimensional space.

To take advantage of the low-rank property as a structural bias for incomplete data [55], we first project the initial features to dense representations by attending to a low-dimensional vector. Specifically, we first randomly initialize a learnable vector which is shared by all nodes with the gradient tractable as the *projector* $\mathbf{P}_{\text{proj}} \in \mathbb{R}^{C \times D'}$, where $C < T$ is the projected dimension. In order to represent the temporal message in a compact form, we then project the input hidden states to the projected space by attending to the query projector:

$$\begin{aligned}\tilde{\mathbf{Z}}_{\text{proj}}^{i,(\ell)} &= \text{SelfAtten}(\mathbf{P}_{\text{proj}}^{(\ell)}, \mathbf{Z}^{i,(\ell)}, \mathbf{Z}^{i,(\ell)}), \\ &= \text{Softmax}\left(\frac{\mathbf{Q}_{\text{proj}}\mathbf{K}_z^\top}{\sqrt{D'}}\right)\mathbf{V}_z,\end{aligned}\quad (9)$$

where $\tilde{\mathbf{Z}}_{\text{proj}}^{i,(\ell)} \in \mathbb{R}^{C \times D'}$ is the projected value. In particular, since the projector \mathbf{P}_{proj} is decoupled from the spatial dimension, the resulted attention map $\text{Softmax}(\mathbf{Q}_{\text{proj}}\mathbf{K}_z^\top/\sqrt{D'}) \in \mathbb{R}^{C \times T}$ can be interpreted as an indicator of how the incomplete time series can be compressed into a compact representation with shorter length, that is, an aggregation of available message. More exposures on the projector will be provided in Section 4.7.4.

$\tilde{\mathbf{Z}}_{\text{proj}}^{i,(\ell)}$ stores the principal temporal patterns within the input data. Then, we can recover the complete series with this compact representation by dispersing the projected

information to all other series by serving as a key:

$$\begin{aligned}\hat{\mathbf{Z}}^{i,(\ell)} &= \text{LayerNorm}(\mathbf{Z}^{i,(\ell)} + \\ &\quad \text{SelfAtten}(\mathbf{Z}^{i,(\ell)}, \mathbf{P}_{\text{proj}}^{(\ell)}, \tilde{\mathbf{Z}}_{\text{proj}}^{i,(\ell)})), \\ \mathbf{Z}^{i,(\ell+1)} &= \text{LayerNorm}(\hat{\mathbf{Z}}^{i,(\ell)} + \\ &\quad \text{FeedForward}(\hat{\mathbf{Z}}^{i,(\ell)})),\end{aligned}\quad (10)$$

where $\mathbf{Z}^{i,(\ell+1)} \in \mathbb{R}^{T \times D'}$ is the imputation by the ℓ -th temporal interaction layer. Since the projector in Eqs. (9) and (10) can be obtained by end-to-end learning and is independent of the order in series, it has the property of data-dependent model in Eq. (5). To indicate how the above process learns the low-rank representation of temporal attention, we develop the following remark.

Remark (Difference between projected attention and temporal attention). *Given the query-key-value matrix $\mathbf{Q}, \mathbf{K}, \mathbf{V} \in \mathbb{R}^{T \times D'}$, the canonical self-attention in the temporal dimension can be expressed in a compact form: $\text{SelfAtten}(\mathbf{Q}, \mathbf{K}, \mathbf{V}) = \sigma(\mathbf{Q}\mathbf{K}^\top)\mathbf{V}$ with the rank $r \leq \min\{T, D'\}$. The two step attentive process in Eqs. (9) and (10) can be equivalently written as an expanded form:*

$$\begin{aligned}\hat{\mathbf{Z}} &= \text{SelfAtten}(\mathbf{Q}, \mathbf{P}, \text{SelfAtten}(\mathbf{P}, \mathbf{K}, \mathbf{V})), \\ &= \sigma(\mathbf{Q}\mathbf{P}^\top)\text{SelfAtten}(\mathbf{P}, \mathbf{K}, \mathbf{V}), \\ &= \sigma(\mathbf{Q}\mathbf{P}^\top)\sigma(\mathbf{P}\mathbf{K}^\top)\mathbf{V}, \\ &\approx \frac{1}{N^2}\mathbf{Q}(\mathbf{P}^\top\mathbf{P})\mathbf{K}^\top\mathbf{V}.\end{aligned}$$

Recall that the projector $\mathbf{P} \in \mathbb{R}^{C \times D'}$ has a small projection dimension C in practice, it can be viewed as a channel-wise matrix factorization to reduce redundancy within each time series. The rank of the projected attention matrix is $r \leq \min\{C, D'\}$, which is theoretically lower than the original rank. It should be noted that the projected attention can guarantee model expressivity by keeping a large hidden dimension D' , while at the same time admitting a low-rank solution by using a small projecting dimension C .

The “projection-reconstruction” process in Eqs. (9) and (10) resemble the low-rank factorization process $\mathbf{X} = \mathbf{U}\mathbf{V}^\top$ [56]. Inflow in Eq. (9) controls the amount of information used to form a dense representation in a lower-dimensional space. Outflow in Eq. (10) determines how hidden states can be reconstructed using only a few projected coordinates. Thus, the projected attention map can be sparse.

This mechanism can also bring about efficiency benefits. The canonical self-attention in Transformers [41] costs $\mathcal{O}(L^2)$ time complexity with the sequence length being L . Although effective in passing messages on all tokens, it is less efficient in long-term series. While the time complexity of the projected attention computation is $\mathcal{O}(TL)$ which scales linearly, it has the potential for inference on longer sequences. In addition, the above computations can be readily extended to multi-head implementations.

3.4 Spatial Interaction with Global Adaptive Graph Convolution

The availability of observed temporal information of a series is not sufficient for full-scale imputation. In some cases, temporal models can struggle with out-of-distribution

(OOD) imputation of the observed data. This OOD problem can be prevalent in fine-grained spatiotemporal data. For example, traffic congestion can result in unexpected local spatial patterns and cause unusual records. Therefore, it is reasonable to exploit the multivariate relationships between series to complement the temporal imputation.

A straightforward way to address this problem is to apply a Transformer block in spatial dimension [8], [52]. Nevertheless, two key concerns prevent the direct use of this technique: (1) *Spurious correlations*: Short-term historical series within a window can be noisy and indistinguishable. Modeling relational structures using pairwise attention or similarity of sparse inputs can generate a high-rank estimation with spurious spatial dependency and redundancy. Such unstable correlations are adverse to the capture of multivariate relationships. On the contrary, the long-term behavior of each series is less sensitive to time-specific events and missing data, and therefore more advantageous to inferring the underlying structures [48], [57], [58]. (2) *High computational cost*: All pairwise attention on large graphs is memory intensive and computationally inefficient for both training and testing in reality.

Consequently, we design a global adaptive graph convolution (GAGC) as an alternative to spatial attention. Recall that the node (sensor) embedding in Eq. (7) not only signifies the identity of each individual but also functions as a low-dimensional abstract of historical series. We then adapt this endogenous representation for a correlation (attention) map by using the trick of adaptive graph convolutions. Formally, we assume that the message passing happens on a fully connected dense graph, and the graph weights are estimated by the pairwise correlating of node embedding:

$$\begin{aligned} \mathbf{Q}_e^{(\ell)} &= \text{Linear}(\mathbf{E}), \mathbf{K}_e^{(\ell)} = \text{Linear}(\mathbf{E}), \\ \mathbf{A}^{(\ell)} &= \text{Softmax} \left(\frac{\mathbf{Q}_e^{(\ell)} \mathbf{K}_e^{(\ell)\top}}{\sqrt{D'}} \right), \end{aligned} \quad (11)$$

where $\mathbf{A}^{(\ell)} \in \mathbb{R}^{N \times N}$ denotes the pairwise correlation score of all sensors, and $\mathbf{Q}_e, \mathbf{K}_e \in \mathbb{R}^{N \times D_{\text{emb}}}$ are linearly projected from the spatiotemporal embedding set $\mathbf{E} = [\bar{\mathbf{e}}^1 \| \bar{\mathbf{e}}^2 \| \dots \| \bar{\mathbf{e}}^N] \in \mathbb{R}^{N \times D_s/T}$, where $\bar{\mathbf{e}}^i$ is the static node embedding averaging over the time span (temporal heads) $\{t : t+T\}$ from Eq. (7). Subsequently, Eq. (11) is involved in the global graph convolution process as follows:

$$\begin{aligned} \tilde{\mathbf{Z}}_t^{(\ell)} &= \text{LayerNorm}(\mathbf{Z}_t^{(\ell)} + \mathbf{A}^{(\ell)} \times \mathbf{Z}_t^{(\ell)}), \\ \mathbf{Z}_t^{(\ell+1)} &= \text{LayerNorm}(\tilde{\mathbf{Z}}_t^{(\ell)} + \text{FeedForward}(\tilde{\mathbf{Z}}_t^{(\ell)})), \end{aligned} \quad (12)$$

where $\mathbf{Z}_t^{(\ell+1)} \in \mathbb{R}^{N \times D'}$ is the imputation at step t in the ℓ -th spatial interaction block. Since Eq. (12) is performed independently at each time step, it can be paralleled using the tensor product. Additionally, \mathbf{E} is independent of temporal information and reflects the inherent features of a sensor.

Given the graph representation over a period $\mathcal{Z} \in \mathbb{R}^{N \times T \times D'}$, the time complexity of obtaining a vanilla attention matrix in spatial dimension costs $\mathcal{O}(N^2 T D')$, while the cost of GAGC is $\mathcal{O}(N^2 D_{\text{emb}})$. Although the actual implementation of GAGC is much faster than the vanilla attention for a long sequence, the overall complexity of GAGC still costs $\mathcal{O}(N^2)$ and can suffer from scalability issues in large sensor graphs. To further reduce the time and memory

complexity, we adopt the approximating normalization trick in [59] to reparameterize Eq. (12).

Observe that the main bottleneck in Eq. (12) happens in the multiplication of two large matrix $\mathbf{Q}_e^{(\ell)}$ and $\mathbf{K}_e^{(\ell)}$, we can reduce the complexity using the associative property of matrix multiplication if we can decouple the softmax function. To this end, we apply the softmax normalization on separate side of the Q-K matrix and approximate $\mathbf{A}^{(\ell)}$ as follows:

$$\mathbf{A}^{(\ell)} \approx \sigma_2(\tilde{\mathbf{Q}}_e^{(\ell)}) \sigma_1(\tilde{\mathbf{K}}_e^{(\ell)})^\top, \quad (13)$$

where $\sigma(\cdot)$ is the abbreviation for softmax, and the subscript denotes the dimension that we perform normalization. $\tilde{\mathbf{Q}}_e^{(\ell)} = \frac{\mathbf{Q}_e^{(\ell)}}{\|\mathbf{Q}_e^{(\ell)}\|_F}$, $\tilde{\mathbf{K}}_e^{(\ell)} = \frac{\mathbf{K}_e^{(\ell)}}{\|\mathbf{K}_e^{(\ell)}\|_F}$ are the scaled Q-K functions to ensure numerical stability. On top of Eq. (13), the proposed GAGC in Eq. (12) can be reformulated as:

$$\begin{aligned} \tilde{\mathbf{Z}}_t^{(\ell)} &= \text{LayerNorm}(\mathbf{Z}_t^{(\ell)} + \sigma_2(\tilde{\mathbf{Q}}_e^{(\ell)}) \sigma_1(\tilde{\mathbf{K}}_e^{(\ell)})^\top \mathbf{Z}_t^{(\ell)}), \\ &= \text{LayerNorm}(\mathbf{Z}_t^{(\ell)} + \sigma_2(\tilde{\mathbf{Q}}_e^{(\ell)}) \left(\sigma_1(\tilde{\mathbf{K}}_e^{(\ell)})^\top \mathbf{Z}_t^{(\ell)} \right)). \end{aligned} \quad (14)$$

By computing the multiplication of $\sigma_1(\tilde{\mathbf{K}}_e^{(\ell)})^\top$ and $\mathbf{Z}_t^{(\ell)}$ at first, the above process admits a $\mathcal{O}(N)$ time complexity, which scales linearly with respect to the number of sensors.

Since \mathbf{E} is decoupled from temporal information, it is robust to missing values and reliable to infer a correlation map for global imputation. The full attention computation on the raw data has the size $\mathbb{R}^{N \times (T \times D')} \times \mathbb{R}^{(T \times D') \times N} \rightarrow \mathbb{R}^{N \times N}$, while the GAGC attention has $\mathbb{R}^{N \times D_{\text{emb}}} \times \mathbb{R}^{D_{\text{emb}} \times N} \rightarrow \mathbb{R}^{N \times N}$. In this sense, the attention map in Eq. (11) is obtained by the low-dimensional abstract of the input data, acting as a low-rank factorized approximation of full attention. We highlight this property by comparing the formulation of GAGC with canonical spatial attention in the following analysis.

Remark (Difference between GAGC and spatial attention). Given a hidden state $\mathcal{Z} \in \mathbb{R}^{N \times T \times D'}$, the self-attention can be computed on the folded matrix $\mathbf{Z} \in \mathbb{R}^{N \times (TD')}$ as $\text{SelfAtten}(\mathbf{Z}, \mathbf{Z}, \mathbf{Z}) = \sigma(\mathbf{Z} \mathbf{W}_Q \mathbf{W}_K^\top \mathbf{Z}^\top) \mathbf{Z} \mathbf{W}_V$. The resulting rank of the attention matrix obeys $r \leq \min\{N, TD'\}$. While the GAGC attention has $\text{SelfAtten}(\mathbf{E}, \mathbf{E}, \mathbf{Z}) = \sigma(\mathbf{E} \mathbf{W}_E) \sigma(\mathbf{E} \mathbf{W}_E)^\top \mathbf{Z} \mathbf{W}_V$. If we ignore the possible rank-increasing effect of softmax [60], the above calculation generates the output with rank $r \leq \min\{N, D_{\text{emb}}\}$. Since the dimension of the node embedding D_{emb} is much smaller than the model dimension D' , the rank of the GAGC attention map has a lower rank than the full attention. In addition, the model still has a large feedforward dimension D' to ensure capacity.

3.5 Fourier Imputation Loss and Learning Strategy

As the deep imputation model is optimized in a self-supervised training manner, in this section we design several task-specific learning strategies to achieve effective training and generalization of imputation models.

3.5.1 Self-Supervised Masked Learning Strategy

First, to evaluate the model, we simulate different observation conditions by removing parts of the raw data to construct incomplete samples based on different missing

Algorithm 1 ImputeFormer - Forward Workflow.

Require: Incomplete time series $\mathbf{X} \in \mathbb{R}^{N \times T}$; input length T ; sensor number N ; node embedding size D_{emb} ; input embedding size D_{in} ; number of spatiotemporal layers L ; masking probability p_{whiten} ; projected dimension size C .

- 1: $\mathbf{X}_{t:t+T} = \text{Mask}(\mathbf{X}_{t:t+T}, p_{\text{whiten}})$ ▷ Training masking with p_{whiten} .
- 2: ▷ Initialize the node embedding and temporal projector.
- 3: $\mathbf{E}_{t:t+T}^i = \text{Parameter}(T, D_{\text{emb}})$, $i = \{1, \dots, N\}$ ▷ $\mathbf{E}_{t:t+T}^i \in \mathbb{R}^{T \times D_{\text{emb}}}$
- 4: $\mathbf{P}_{\text{proj}}^{(\ell)} = \text{Parameter}(C, D')$, $\ell = \{1, \dots, L-1\}$ ▷ $\mathbf{P}_{\text{proj}} \in \mathbb{R}^{C \times D'}$
- 5: ▷ Expand the last dimension to get the initial state.
- 6: $\mathbf{Z}_{t:t+T}^{(0)} = \text{MLP}(\text{Unsqueeze}(\mathbf{X}_{t:t+T}, \text{dim}=-1))$ ▷ $\mathbf{Z}_{t:t+T}^{(0)} \in \mathbb{R}^{N \times T \times D_{\text{in}}}$
- 7: ▷ Spatiotemporal input embedding.
- 8: $\mathbf{Z}_{t:t+T}^{i,(1)} = \text{Concat}(\mathbf{Z}_{t:t+T}^{i,(0)}; \mathbf{U}_{t:t+T}; \mathbf{E}_{t:t+T}^i, \text{dim}=-1)$, $i = \{1, \dots, N\}$ ▷ $\mathbf{Z}_{t:t+T}^{i,(1)} \in \mathbb{R}^{N \times T \times D'}$
- 9: **for** ℓ **in** $\{2, \dots, L\}$: ▷ Run through ImputeFormer blocks.
- 10: ▷ Projected attention is applied in the time dimension for temporal imputation.
- 11: $\mathbf{Z}^{i,(\ell-1)} = \text{TemporalInteraction}(\mathbf{Z}^{i,(\ell-1)}, \mathbf{P}_{\text{proj}}^{(\ell-1)})$, $i = \{1, \dots, N\}$ ▷ $\mathbf{Z}^{i,(\ell-1)} \in \mathbb{R}^{T \times D'}$, $\mathbf{P}_{\text{proj}}^{(\ell-1)} \in \mathbb{R}^{C \times D'}$
- 12: ▷ Global adaptive graph convolution is applied in the space dimension for spatial imputation.
- 13: $\mathbf{Z}_t^{(\ell)} = \text{SpatialInteraction}(\mathbf{Z}_t^{(\ell-1)}, \mathbf{E}_t)$, $t = [t, \dots, t+T]$ ▷ $\mathbf{Z}_t^{(\ell)} \in \mathbb{R}^{N \times D'}$, $\mathbf{E}_t \in \mathbb{R}^{N \times D_{\text{emb}}}$
- 14: **End for**
- 15: ▷ Readout and dimension reduction layer.
- 16: $\hat{\mathbf{X}}_{t:t+T} = \text{Squeeze}(\text{MLP}(\mathbf{Z}^L))$ ▷ $\hat{\mathbf{X}}_{t:t+T} \in \mathbb{R}^{N \times T}$
- 17: **Return** $\hat{\mathbf{X}}_{t:t+T}$ ▷ Return the final imputation result $\hat{\mathbf{X}}_{t:t+T}$.

rates (p_{missing}). The evaluation metrics are then calculated on these simulated missing points. We use a masking indicator $\mathbf{M}_{\text{missing}}$ to denote these locations in which the unobserved (missing) values are marked as 1, observed as 0.

Second, as shown in Eq. (1), an effective self-supervised training scheme is needed. During model training, we further randomly whiten a proportion of incomplete observations (p_{whiten}) to create supervised samples. This operation ensures the generalizability of the imputation model (see Section 4.6.2). We use a masking indicator $\mathbf{M}_{\text{whiten}}$ to denote these locations in which the masked values are marked as 1, others as 0. Note that the reconstruction (supervision) loss is only calculated on these manually whitened points, and models are forbidden to have access to the masked missing points used for evaluation (i.e. $\mathbf{M}_{\text{missing}}$). Therefore, the reconstruction loss of our model is a straightforward ℓ_1 loss on the output of the final readout layer:

$$\mathcal{L}_{\text{recon}} = \frac{1}{NT} \sum \|\mathbf{M}_{\text{whiten}} \odot (\hat{\mathbf{X}} - \mathbf{Y})\|_1, \quad (15)$$

where $\hat{\mathbf{X}}$ is the final imputation, and \mathbf{Y} is the complete data used for training.

3.5.2 Fourier Sparsity Regularization

The design of the loss function is of vital importance for imputation models. Previous studies proposed adopting accumulated and hierarchical loss [18], [19], [20] to improve the supervision of layerwise imputation. However, we argue that hierarchical loss is not necessary and may generate a biased model as well as overfitting. Instead, we propose a new Fourier imputation loss (FIL) as an inductive bias for the time series imputation task.

As discussed above, spatiotemporal data such as traffic data usually features a low-rank property in the time domain [6], [9], [10]. In other words, we can obtain a reasonable imputation by constraining the rank of the estimated

spatiotemporal tensor in the time domain. To impose a low-rank constraint on the solution of the imputation problem, traditional low-rank models usually design an objective to reduce the approximate rank function. However, directly optimizing the rank of the tensor or matrix is challenging [55], as it includes some non-trivial or non-differentiable computations, such as truncated singular value decomposition (SVD). And the SVD of a $N \times T$ matrix costs $\mathcal{O}(\min\{N^2T, NT^2\})$ complexity [61], which can become a bottleneck when integrated with deep models. Fortunately, we can simplify this process using the following lemma.

Lemma (Equivalence between convolution nuclear norm and Fourier ℓ_1 norm [62], [63]). *Given a smooth or periodic time series $\mathbf{x} \in \mathbb{R}^T$, its circulant (convolution) matrix $\mathcal{C}(\mathbf{x}) \in \mathbb{R}^{T \times T}$ reflects the Tucker low-rankness. This property can be revealed by using the Discrete Fourier Transform (DFT) [61]. Let the DFT matrix be $\mathbf{U} \in \mathbb{C}^{T \times T}$, then the DFT is achieved by:*

$$\begin{aligned} \text{DFT}(\mathbf{x}) &= \mathbf{U}\mathbf{x} = \mathbf{U}(\mathcal{C}(\mathbf{x})[:, 0]), \\ &= (\mathbf{U}\mathcal{C}(\mathbf{x}))[:, 0], \end{aligned}$$

As circulant matrix can be diagonalized by $\mathcal{C}(\mathbf{x}) = \mathbf{U}^H \text{diag}(\sigma_1, \sigma_2, \dots, \sigma_T) \mathbf{U}$ and \mathbf{U} is a unitary matrix with the first column being all ones, we have:

$$\begin{aligned} \mathbf{U}\mathcal{C}(\mathbf{x})[:, 0] &= (\text{diag}(\sigma_1, \sigma_2, \dots, \sigma_T) \mathbf{U})[:, 0], \\ &= [\sigma_1, \sigma_2, \dots, \sigma_T]^T. \end{aligned}$$

Therefore, we have $\|\text{DFT}(\mathbf{x})\|_0 = \|[\sigma_1, \sigma_2, \dots, \sigma_T]^T\|_0 = \text{rank}(\mathcal{C}(\mathbf{x}))$, and $\|\text{DFT}(\mathbf{x})\|_1 = \|\mathcal{C}(\mathbf{x})\|_*$.

This lemma means that we can efficiently obtain the singular values through DFT. The ℓ_0 norm is exactly the matrix rank and the ℓ_1 norm is equal to the nuclear norm $\|\mathcal{C}(\mathbf{x})\|_*$. Since the nuclear norm is widely adopted to serve as a convex surrogate of matrix rank, we can equivalently achieve this goal by directly optimizing the Fourier ℓ_1 norm.

Considering the above equivalence, we can develop a sparsity-constrained loss function in the frequency domain:

$$\begin{aligned} \bar{\mathbf{X}} &= \mathbf{M}_{\text{missing}} \odot \hat{\mathbf{X}} + (1 - \mathbf{M}_{\text{missing}}) \odot \mathbf{Y}, \\ \mathcal{L}_{\text{FIL}} &= \frac{1}{NT} \sum \|\text{Flatten}(\text{FFT}(\bar{\mathbf{X}}, \text{dim} = [0, 1]))\|_1, \end{aligned} \quad (16)$$

where $\text{FFT}(\cdot)$ is the Fast Fourier Transform (FFT), $\text{Flatten}(\cdot) : \mathbb{R}^{N \times T} \rightarrow \mathbb{R}^{NT}$ rearranges the tensor form and $\|\cdot\|_1$ is the vector ℓ_1 norm. Since the spatiotemporal matrix can be regarded as a special RGB image from a global viewpoint, it also features a sparse Fourier spectrum in the space dimension [62]. We apply the FFT on both the space and time axes and then flatten it into a long vector. \mathcal{L}_{FIL} is in fact a unsupervised loss that encourages the imputed values to be naturally compatible with the observed values globally. Note that the ℓ_1 norm computes the mode of the complex vector, ensuring operation in the real domain.

Finally, the total loss function is formulated as:

$$\mathcal{L} = \mathcal{L}_{\text{recon}} + \lambda \mathcal{L}_{\text{FIL}}, \quad (17)$$

where λ is a weight hyperparameter. It is worth commenting that the two loss functions complement each other: $\mathcal{L}_{\text{recon}}$ prompts the model to reconstruct the masked observations as precisely as possible in the space-time domain and \mathcal{L}_{FIL} powers the model to generalize on unobserved points with regularization on the spectrum. This makes *ImputeFormer* work effectively in highly sparse observations.

In summary, the complete forward workflow of *ImputeFormer* is briefly presented in Algorithm 1.

TABLE 1: Results (in terms of MAE) on traffic speed data.

Models	Point missing		Block missing	
	PEMS-BAY	METR-LA	PEMS-BAY	METR-LA
Average	5.45	7.52	5.48	7.43
MICE [26]	2.82	2.89	2.36	2.73
TRMF [28]	2.10	3.51	2.09	3.36
LRTC-AR [12]	0.94	2.14	4.05	5.35
Bi-MPGRU	0.72	2.00	1.41	2.33
rGAIN [32]	1.90	2.81	2.21	2.95
BRITS [16]	1.84	2.42	1.91	2.40
SAITS [19]	1.33	2.25	1.58	2.32
Transformer [41]	0.76	2.18	1.69	3.58
ST-Transformer	0.75	2.19	1.71	3.58
TIDER [13]	1.43	2.68	2.46	4.95
TimesNet [64]	1.47	2.93	2.73	4.79
GRIN [18]	0.68	1.91	1.20	2.08
SPIN [20]	0.79	1.93	1.13	2.02
ImputeFormer	0.64 5.9% ↓	1.80 5.8% ↓	0.95 15.9% ↓	1.86 7.9% ↓

4 EMPIRICAL EVALUATIONS

In this section, we benchmark the proposed model on several well-known spatiotemporal datasets, comparing it with state-of-the-art baselines, as well as evaluating its generality on different scenarios. Then comprehensive analysis and model interpretations are provided for discussion. Our implementations and reproducible experimental results will be public at: <https://github.com/tongnie/ImputeFormer>.

4.1 Datasets and Experimental Settings

4.1.1 Benchmark datasets

We adopt heterogeneous spatiotemporal datasets to evaluate the imputation performance. Brief statistical information about the benchmark datasets is summarized in Tab. 3.

Traffic Speed Data: Our experiments include two commonly used traffic speed datasets, named METR-LA and PEMS-BAY. METR-LA contains spot speed data from 207 loop sensors over a period of 4 months from Mar 2012 to Jun 2012, located at the Los Angeles County highway network. PEMS-BAY records 6 months of speed data from 325 static detectors in the San Francisco South Bay Area.

Traffic Volume Data: We introduce four traffic volume datasets, including PEMS03, PEMS04, PEMS07, and PEMS08. PEMS0X contains the highway traffic volume information in California, which is collected by the Caltrans Performance Measurement System (PeMS) [65] and aggregated into 5-minute interval for experiments. Similar to METR-LA and PEMS-BAY, PEMS0X also includes a adjacency graph calculated by the physical distance between sensors.

Energy and Environmental Data: Four additional datasets are selected to evaluate the generality of models, including: (1) *Solar*: solar power production records from 137 synthetic PV farms in Alabama state in the year 2006, which are sampled every 10 minutes; (2) *CER-EN*: smart meters measuring energy consumption from the Irish Commission for Energy Regulation Smart Metering Project [66]. Following the setting in [18], we select 435 time series aggregated at 30 minutes for evaluation. (3) *AQI*: PM2.5 pollutant measurements collected by 437 air quality monitoring stations in 43 Chinese cities from May 2014 to April 2015 with the aggregation interval of 1 hour. Note that raw AQI data contains nearly 26% missing data. (4) *AQI36*: a subset of AQI data which contains 36 sensors in Beijing district.

4.1.2 Experimental Settings and Baseline Methods

Missing patterns: For traffic, solar and CER-EN data, we consider two scenarios discussed in [18], [20]: (1) *Point missing*: randomly remove observation points with 25% probability; (2) *Block missing*: randomly drop 5% of the available data and at the same time simulate a sensor failure lasting for $\mathcal{L} \sim \mathcal{U}(12, 48)$ steps with 0.15% probability. We keep the above missing rates the same as in the previous works [18], [20] to benchmark our model. For supplementary experiments, we also evaluated the performance under sparser conditions. For example, the block missing with 10% probability corresponds to a total missing rate of $\approx 90 \sim 95\%$ in our case. Note that matrix or tensor models can only handle in-sample imputation, where the observed training data and the evaluating data are in the same time period. Whereas, deep imputation models can work in an out-of-sample scenario [18] where the training and evaluating sequences are disjoint. In our experiments, we adopt the out-of-sample routine for deep imputation models and in-sample manner for other models.

Baseline Methods: We compare our model with state-of-the-art deep learning models and analytical methods in the related literature. For statistical and optimization models, we consider: (1) Observation average (*Average*); (2) Temporal regularized matrix factorization (TRMF) [28];

TABLE 2: Results (in terms of MAE) on PEMS03, PEMS04, PEMS07 and PEMS08 traffic volume benchmarks.

Models	Point missing				Block missing			
	PEMS03	PEMS04	PEMS07	PEMS08	PEMS03	PEMS04	PEMS07	PEMS08
Average	85.30	103.61	122.35	89.51	85.56	103.82	123.05	89.42
MICE	20.07	28.60	37.11	30.26	21.90	32.45	37.20	26.66
TRMF	18.80	24.34	29.06	20.27	18.71	24.47	29.42	19.80
Bi-MPGRU	11.23	15.84	15.66	11.90	13.87	19.81	21.12	15.89
rGAIN	13.32	22.86	24.41	16.33	14.85	23.26	26.69	27.12
BRITS	12.74	20.00	23.97	15.78	12.93	19.80	23.26	16.37
SAITS	12.40	20.23	22.81	15.12	12.43	20.35	22.82	16.80
Transformer	12.04	16.76	16.86	12.58	24.07	29.63	33.14	25.61
ST-Transformer	11.44	16.22	15.84	12.10	23.55	29.17	32.14	24.67
TimesNet	14.99	20.40	22.00	16.53	44.85	51.05	60.90	45.78
GRIN	10.31	16.25	11.90	12.33	12.28	23.23	16.04	19.69
SPIN	12.85	18.96	17.61	15.02	14.68	19.85	16.99	16.81
ImputeFormer	8.23 20.2% ↓	14.92 5.8% ↓	11.38 4.4% ↓	11.01 7.5% ↓	9.02 26.5% ↓	16.83 15.0% ↓	13.82 13.8% ↓	12.50 21.3% ↓

TABLE 3: Statistics of benchmark datasets.

Datasets	Type	Steps	Nodes	Interval
METR-LA	Traffic speed	34,272	207	5 min
PEMS-BAY	Traffic speed	52,128	325	5 min
PEMS03	Traffic volume	26,208	358	5 min
PEMS04	Traffic volume	16,992	307	5 min
PEMS07	Traffic volume	28,224	883	5 min
PEMS08	Traffic volume	17,856	170	5 min
SOLAR	Power production	52,560	137	10 min
CER-EN	Energy consumption	8,868	435	30 min
AQI	Air pollutant	8,760	437	60 min
AQI36	Air pollutant	8,760	36	60 min

(3) Low-rank autoregressive tensor completion (LRTC-AR) [12]; (4) MICE [26]. For deep imputation models, we select several competitive baselines: (1) SPIN [20]: sparse spatiotemporal attention model with state-of-the-art imputation performance; (2) GRIN [18] message-passing-based bidirectional RNN model with competitive performance; (3) SAITS [19]: Temporal Transformer model with diagonally masked attention; (4) BRITS [16]: bidirectional RNN model for imputation; (5) rGAIN [32]: GAIN model with bidirectional recurrent encoder and decoder; (6) Transformer/ST-Transformer [41]: canonical Transformer model with self-attention in temporal or spatial-temporal dimensions; (7) TiDER [13]: matrix factorization with disentangled neural representations; (8) TimesNet [64]: 2D convolution-based general time series analysis model; (9) BiMPGRU: a bidirectional RNN based GCN model which is similar to DCRNN [67].

Model Implementations: We build our model and other baselines based on the SPIN repository¹ using PyTorch. All experiments are conducted on a single NVIDIA RTX A6000 (48 GB) GPU. For the hyperparameters of ImputeFormer, we set the hidden size to 256, the input projection size to 32, the node embedding size to 64, the projected size to 8, and the number of spatiotemporal layers to 3. The settings of other baselines can refer to the SPIN repository or our open-source implementations. Additionally, we keep the same training, validation, and evaluation split as [18], [20] and

report the metrics on the masked evaluating points.

4.2 Results on Traffic Benchmarks

The imputation results on traffic speed and volume data are given in Tab. 1 and 2. As can be seen, ImputeFormer consistently achieves the best imputation accuracy in all traffic benchmarks. Two strong competitors GRIN and SPIN show promising results on traffic speed datasets, which are align with the results of their respective papers [18], [20]. However, their performances are inferior on volume datasets, and are surpassed by simple baselines such as ST-Transformer and Bi-MPGRU. Compared to deep imputation models, pure low-rank methods such as matrix factorization and tensor completion are less effective due to limited model capacity. As for missing patterns, the structured block missing is more challenging than the point missing pattern. For instance, the vanilla Transformer is competitive in the point missing case, while it is ineffective in block missing case. Generally, ImputeFormer outperforms others by a large margin in this tricky scenario.

4.3 Results on Other Benchmarks

By exploiting the underlying low-rank structures, ImputeFormer can serve as a general missing data estimator in a variety of spatiotemporal tasks. To demonstrate the versatility of the proposed architecture, we perform experiments on other data sources. Specifically, we evaluate our model on datasets with missing observations and without predefined graphs. Results are given in Tab. 4.

It is observed that ImputeFormer also exhibits superiority in other spatiotemporal datasets beyond traffic data. In particular, the correlation of solar stations cannot be described by physical distance and can be inferred from the data. However, after comparing the performance of Transformer, ST-Transformer, SAITS, and ImputeFormer, it can be concluded that direct attention computations on both temporal and spatial dimensions are less beneficial than low-rank attention in our model. Furthermore, the spatial correlation of energy production is less pronounced. The canonical attention on the spatial axis can be redundant and generate spurious correlations. The use of GAGC can alleviate this issue to some extent.

1. <https://github.com/Graph-Machine-Learning-Group/spin>

TABLE 4: Results (in terms of MAE) on AQI and Solar benchmarks. For Solar data, we compare the performances of baselines that are independent of the predefined graphs.

Models	SOLAR		CER-EN		Simulated faults	
	Point Missing	Block Missing	Point Missing	Block Missing	AQI-36	AQI
Average	7.60	7.56	0.583	0.596	61.81	43.78
MICE	1.59	1.58	0.535	0.555	38.90	29.12
TRMF	2.44	2.35	0.557	0.559	41.91	27.67
Bi-MPGRU	N.A.	N.A.	0.247	0.349	12.02	15.41
rGAIN	1.52	1.64	0.418	0.440	15.69	22.13
BRITS	1.28	1.34	0.351	0.366	14.74	20.72
SAITS	0.98	1.25	0.341	0.368	19.79	21.09
Transformer	2.19	3.58	0.254	0.353	14.99	17.04
ST-Transformer	2.17	3.57	0.251	0.351	13.27	18.55
TIDER	2.84	3.87	0.336	0.377	32.85	18.11
TimesNet	2.93	4.73	0.328	0.460	32.30	28.99
GRIN	N.A.	N.A.	0.235	0.341	12.08	14.51
SPIN	N.A.	N.A.	OOM	OOM	11.89	14.31
ImputeFormer	0.51 48.0% ↓	0.89 28.8% ↓	0.236 0.4% ↑	0.296 13.2% ↓	11.58 2.6% ↓	13.40 6.4% ↓

TABLE 5: Ablations on ImputeFormer. We remove or replace specific components and report corresponding results.

Variation	Component		PEMS08		METR-LA	
	Spatial	Temporal	Point	Block	Point	Block
ImputeFormer	Attention	Attention	11.24	12.86	1.80	1.88
Replace	Attention	MLP	16.95	17.11	2.39	2.28
	MLP	Attention	12.84	17.42	2.20	2.92
	MLP	MLP	34.72	34.41	5.80	5.79
w/o	Attention	w/o	17.06	17.13	2.39	2.28
	w/o	Attention	12.87	17.44	2.21	2.93
Loss function	w/o FIL		11.37	12.97	1.85	1.93
	Hierarchical loss		11.35	13.07	1.84	1.92

4.4 Ablation Study

To justify the rationale of model designs, we conduct ablation studies on the model structure. Particularly, we examine the following three aspects of ImputeFormer:

- 1) Temporal blocks: we replace the temporal interaction module with MLP or directly remove it;
- 2) Spatial blocks: we replace the spatial interaction module with MLP or directly remove it;
- 3) Loss function: We remove the FIL or replace it with a hierarchical loss used in [19], [20].

We adopt the PEMS08 and METR-LA datasets to evaluate each variation. And other experimental settings are consistent with section 4.2. Results are shown in Tab. 5. Several intriguing findings can be observed in this table: (1) After removing any of the temporal and spatial attention modules, the performance degenerates substantially; Especially, the spatial interaction contributes to the inference of block missing patterns significantly, while the temporal modules are crucial for point missing scenarios. (2) The incorporation of MLP benefits little for the imputation, which validates our argument in section 3.2. (3) Compared to hierarchical loss on the supervised points, FIL generalizes on the unobserved points and effectively reduce the estimation errors.

4.5 Model Efficiency

Demonstrating high efficiency in the class of Transformers and RNNs models is also a significant superiority of ImputeFormer. We therefore evaluate the computational efficiency of different architectures. To give an unbiased comparison, we set the batch size to 32 and the hidden size to 128 for all models. The results are shown in Fig. 4. Intuitively, it can be seen that ImputeFormer exhibits high training efficiency. Thanks to the low-rank design philosophy, our architecture is approximately 15 times faster than the state-of-the-art Transformer baseline (SPIN). It is also cost-effective in GPU memory consumption.

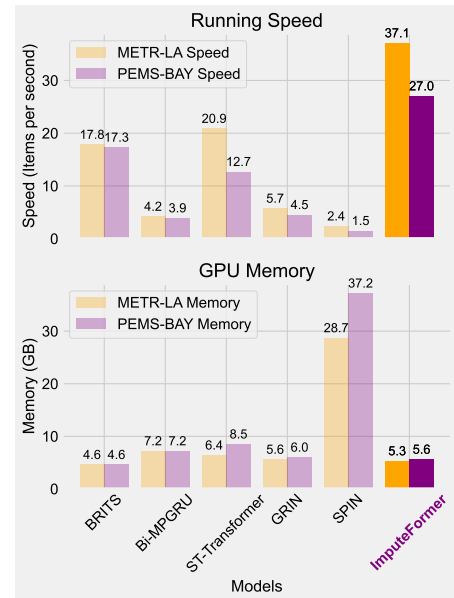


Fig. 4: Comparison of computational efficiency.

4.6 Further Discussions

To help better understand the superiority of our model and demonstrate its generality, this section provides more

discussion and analysis, including training techniques, different inference scenarios, and result interpretations.

4.6.1 Random Masking in Training

The random masking strategy is utilized to create supervised samples for model training. Therefore, the distribution of masking samples of training data and missing observations of testing data should be close to ensure good performance, which is recognized in our previous work [40]. However, it can be difficult to know exactly the missing patterns or missing rates in advance in many real-world scenarios. Therefore, a proper masking strategy is of vital importance. To evaluate the impact of the masking rate in training data, we further consider four different masking strategies during model training: the masking rates are set to 0.25, 0.5, 0.75, and a combination of them [0.25, 0.5, 0.75] respectively. We use the PEMS03 data as a demonstration.

TABLE 6: Results on PEMS03 data (25% point missing) with various masking strategies.

Models	Masking Probability			
	25%	50%	75%	Combination
Bi-MPGRU	11.30	11.52	12.20	11.48
BRITS	13.06	13.86	16.06	13.70
SAITS	12.42	16.13	21.63	12.61
ST-Transformer	11.19	11.43	12.22	11.39
GRIN	9.55	9.74	10.39	9.72
SPIN	11.08	11.21	13.85	12.04
ImputeFormer	7.66	8.16	11.44	8.45

TABLE 7: Results on PEMS03 data (block missing) with various masking strategies.

Models	Masking Probability			
	25%	50%	75%	Combination
Bi-MPGRU	13.32	13.36	13.96	13.33
BRITS	12.26	13.01	15.58	12.63
SAITS	12.35	15.73	20.14	12.32
ST-Transformer	23.51	23.76	23.90	23.26
GRIN	11.94	12.05	12.68	11.99
SPIN	13.10	13.68	13.84	13.97
ImputeFormer	8.89	9.23	16.96	8.80

As shown in Tabs. 6 and 7, most models perform best when the masking rate is close to the missing rate in the point missing scenario (e.g., 25%). However, when the missing rate is unclear due to randomness within the failure generation process, such as the block missing pattern, the combination strategy is more advantageous. For example, Transformers including ST-Transformer, SAITS, and ImputeFormer can benefit from this strategy. More importantly, such a hybrid masking method enables the model to work successfully on varying observation rates during inference.

4.6.2 Inference under Different Missing Rates

Deep imputation models are subject to the distribution shift problem between training and testing datasets. A desirable characteristic is that a model can deal with different missing

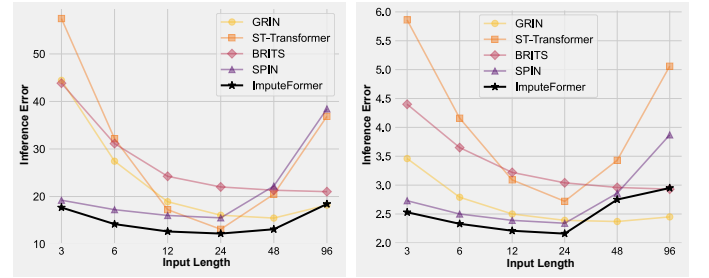
patterns during inference. Therefore, we consider a challenging scenario in which a model is trained with a fixed missing rate but evaluated on different scenarios with varying missing rates. This constructs a zero-shot transfer evaluation. It is noteworthy in Tab. 8 that both ImputeFormer and SPIN are more robust than other baselines in these scenarios. The RNNs and vanilla Transformer models can overfit the training data with a fixed data missing pattern, thereby showing inferior generalization ability.

TABLE 8: Inference under varying missing rate with a single trained model (Zero-shot).

Models	PEMS08			METR-LA		
	Missing rate			Missing rate		
	50%	75%	95%	50%	75%	95%
BRITS	17.21	22.01	52.78	2.61	3.04	5.11
SAITS	16.03	31.32	83.79	2.44	3.37	6.80
ST-Transformer	11.65	13.11	39.95	2.32	2.72	5.16
GRIN	13.25	16.06	42.61	2.06	2.39	4.07
SPIN	15.13	15.51	18.30	2.11	2.34	3.03
ImputeFormer	11.52	12.18	17.35	1.96	2.17	2.79

4.6.3 Inference with Varying Sequence Length

In reality, the imputation model can confront with time series with different lengths and sampling frequencies. As the Transformer model has the ability to work on inputs with different sequence lengths, we can adopt a well-trained model to perform inference on varying sequence length. Results are shown in Fig. 5. It is obvious that ImputeFormer can readily generalize to input sequences with different lengths and more robust than other models.



(a) PEMS08

(b) METR-LA

Fig. 5: Inference under different lengths of input sequence with a single trained model (zero-shot).

4.6.4 Dealing with Highly Sparse Observation

To evaluate the performance of our method on highly sparse data, we further train and test ImputeFormer on scenarios with lower observation rates. Results are shown in Tab. 9.

Generally speaking, both Transformer- and RNN-based architectures are susceptible to sparse training data. Due to the low-rank constraints on both neural representations and the loss function, ImputeFormer is relatively more robust with highly sparse data. Since the attention matrices in SPIN are calculated only on observed points, it is more stable than other baselines. But our model consistently achieves lower imputation errors.

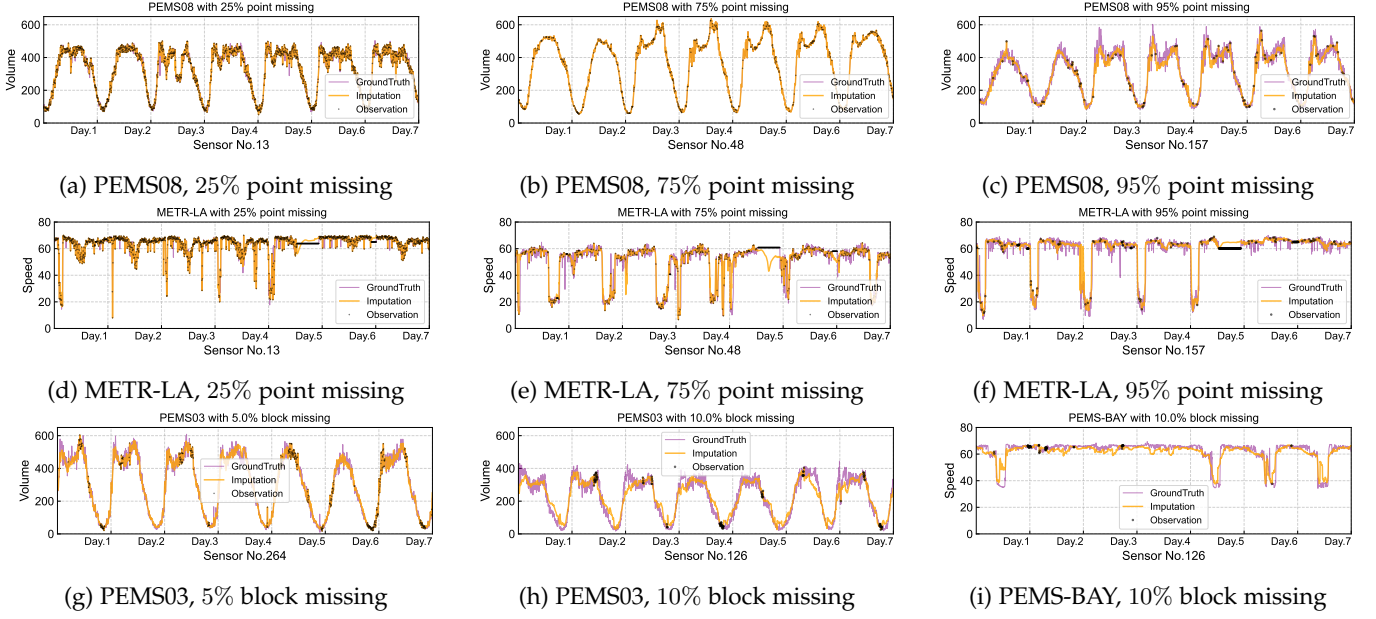


Fig. 6: Visualization examples of imputation for traffic speed and volume data under different missing patterns.

TABLE 9: Results on PEMS08 data (point missing) with sparse observations (Training from scratch).

Models	Missing rate			
	60%	70%	80%	90%
BRITS	18.60	19.75	21.44	24.17
SAITS	17.53	18.24	19.39	21.27
ST-Transformer	13.67	14.32	15.86	23.98
GRIN	14.04	15.01	17.26	25.47
SPIN	13.64	14.30	15.19	17.13
ImputeFormer	12.57	13.17	13.98	15.94

4.7 Case Studies

To enhance the interpretability of `ImputeFormer`, we provide several case studies to discuss the functionality of spatial-temporal interaction blocks and visualizations of imputation results.

4.7.1 Imputation Visualization

We provide several visualization examples of the traffic datasets in Fig. 6. As evidenced by Fig. 6, `ImputeFormer` can generate reasonable estimations for missing values by learning the inherent structures of multivariate time series. Previous studies have discovered that low-rank imputation models can cause oversmoothing estimation [10], [12]. Due to the representation power of deep architecture, our model can provide a detailed reconstruction. In particular, although only limited temporal information is available for reference in the block missing case, the model can resort to the node embedding as the query to spatial relations.

4.7.2 Spectrum Analysis

To corroborate our hypothesis that `ImputeFormer` has the merits of both deep learning and low-rank methods, we analyze the singular value spectrum of the imputations of different models. Fig. 7 shows the cumulative singular value

distribution of different competing models. `ImputeFormer` has a close singular cumulative distribution to the complete data, and the first 85 singular values can account for 80% of the energy. There exist two additional interesting observations: (1) Deep learning models without explicit low-rank modeling such as the canonical Transformer can downplay the role of the first few significant singular values; (2) Pure low-rank models such as matrix factorization generate an over-squashing imputation that too much energy is constrained to the first part of spectrum. Therefore, we can ascribe the desirable performance of `ImputeFormer` to the good balance of significant signals and high-frequency noise.

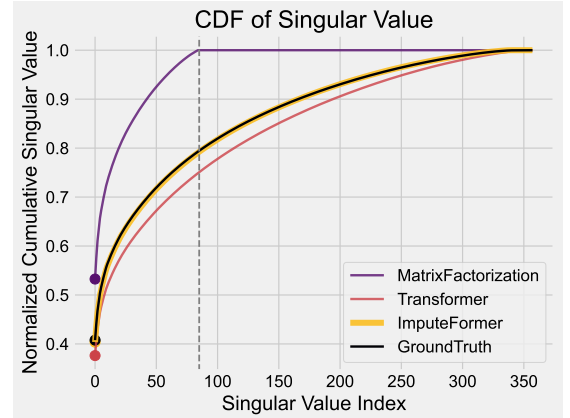


Fig. 7: Cumulative distribution function of singular values. We compare the normalized cumulative singular values of different methods in PEMS03 data.

4.7.3 Explanations on Spatial Embedding

As stated above, the node embedding serves as a compact representation of the incomplete signal of a series (sensor). We use an implicit learning trick to obtain this embedding.

Fig. 8 (a) displays the t-SNE visualization of each node embedding with two projected coordinates. The embeddings tend to form clusters, and different clusters are apart from others. This phenomenon is in accordance with highway traffic sensor systems that proximal sensors share similar readings within a time period. From another perspective, we analyze the singular value spectrum of the PEMS08 data in Fig. 8 (b). The complete data shows a significant low-rank property, but the singular values of corrupted data dramatically expand. In contrast, the learnable node embedding also obeys a similar low-rank distribution, which can act as a dense surrogate for each sensor.

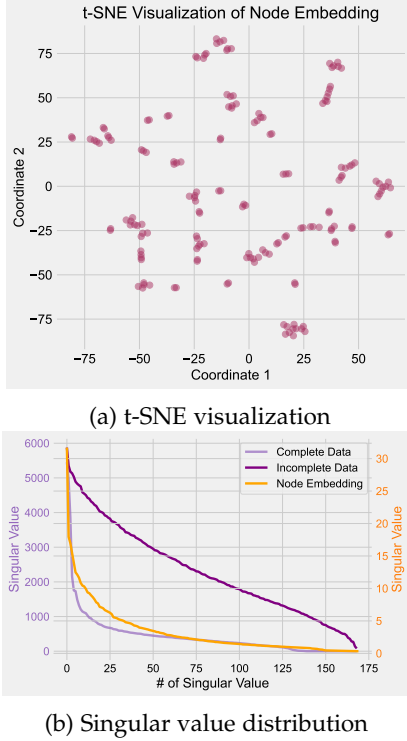


Fig. 8: Explanations on node (sensor) embedding using PEMS08 data. (a) Two-dimensional t-SNE visualization of each node embedding. (b) Singular spectrum of complete data, incomplete observations, and node embedding.

Taking it a step further, we analyze the multivariate attention map obtained by correlating the node embedding in Fig. 9. To obtain a referable correlation map of complete data, we calculate the absolute value of Pearson coefficient in Fig. 9 (c). It is evident that as the GAGC layers become deeper, the learned attention maps approach the actual ones. Nevertheless, the incomplete data produce noisy correlations with little useful information.

4.7.4 Explanations on Temporal Projector

Recall that the temporal projector is designed to reduce redundancy in the representation of incomplete series. By projecting the whole series into a compact state, the projected attention in Eqs. (9) and (10) can filter effective information for reconstruction. To illustrate this process, the inflow and outflow attention maps are given in Figs. 10 and 11.

It can be observed that these matrices quantify how the information of incomplete hidden states is compressed

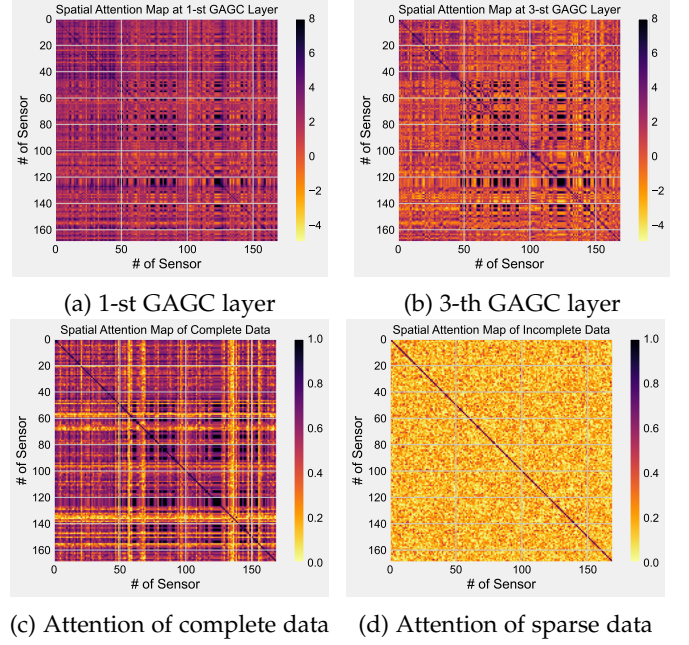


Fig. 9: Multivariate attention maps of PEMS08 data. (a) Attention in the 1-st GAGC layer. (b) Attention in the 3-th GAGC layer. (c) Correlation map of the complete data. (d) Correlation map of incomplete data.

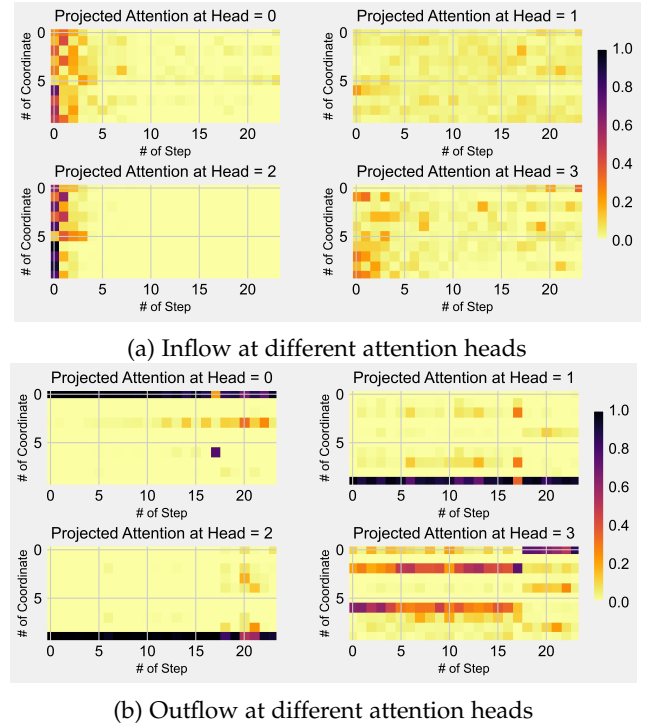


Fig. 10: Inflow and outflow of temporal information in the projected attention layer. The x-axis is the number of time steps, and the y-axis is the number of projected coordinates.

into compact representations and then is recovered to the complete states. Fig. 10 (a) shows that only a fraction of the information is directed towards the projector, while different attention heads can provide varying levels of information density. Meanwhile, Fig. 10 (b) denotes that a small number of coordinates can reconstruct useful neural representations for subsequent imputation.

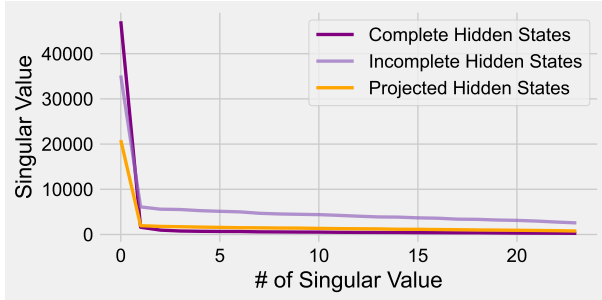


Fig. 11: Singular value distribution of different hidden representations in the temporal attention layer.

We further examine the singular value distribution of different hidden representations in the last temporal attention layer. As evidenced by Fig. 11, after flow through the projected attention layer, the hidden states have lower singular values than the incomplete inputs and are closer to the complete representations.

5 CONCLUSION

This paper demonstrates a low rankness-induced Transformer model termed *ImputeFormer* to address the missing spatiotemporal data imputation problem. Taking advantage of the low-rank factorization, we design projected temporal attention and global adaptive graph convolution to incorporate structural priors into the Transformer model. Furthermore, a Fourier imputation loss is developed to regularize the solution spectrum. Evaluation results on various benchmarks indicate that *ImputeFormer* not only consistently achieves state-of-the-art imputation accuracy, but also exhibits high computational efficiency, generalizability across various datasets, versatility for different scenarios, and interpretability of the results. Therefore, we believe that *ImputeFormer* has the potential to advance research on spatiotemporal data for general imputation tasks. Future work can adopt *ImputeFormer* to achieve time series representation learning task [42] and explore the multipurpose pretraining problem for time series [68].

ACKNOWLEDGMENTS

This research was sponsored by the National Natural Science Foundation of China (52125208), the Science and Technology Commission of Shanghai Municipality (No. 22dz1203200), and the National Natural Science Foundation of China's Young Scientists Fund (52302413).

REFERENCES

- [1] Y. Duan, Y. Lv, Y.-L. Liu, and F.-Y. Wang, "An efficient realization of deep learning for traffic data imputation," *Transportation research part C: emerging technologies*, vol. 72, pp. 168–181, 2016.
- [2] X. Chen, Z. He, and L. Sun, "A bayesian tensor decomposition approach for spatiotemporal traffic data imputation," *Transportation research part C: emerging technologies*, vol. 98, pp. 73–84, 2019.
- [3] Y. Chen, Y. Lv, and F.-Y. Wang, "Traffic flow imputation using parallel data and generative adversarial networks," *IEEE Transactions on Intelligent Transportation Systems*, vol. 21, no. 4, pp. 1624–1630, 2019.
- [4] Y. Zheng, X. Yi, M. Li, R. Li, Z. Shan, E. Chang, and T. Li, "Forecasting fine-grained air quality based on big data," in *Proceedings of the 21th ACM SIGKDD international conference on knowledge discovery and data mining*, 2015, pp. 2267–2276.
- [5] X. Chen, C. Zhang, X.-L. Zhao, N. Saunier, and L. Sun, "Nonstationary temporal matrix factorization for multivariate time series forecasting," *arXiv preprint arXiv:2203.10651*, 2022.
- [6] X. Chen, J. Yang, and L. Sun, "A nonconvex low-rank tensor completion model for spatiotemporal traffic data imputation," *Transportation Research Part C: Emerging Technologies*, vol. 117, p. 102673, 2020.
- [7] H. Li, M. Li, X. Lin, F. He, and Y. Wang, "A spatiotemporal approach for traffic data imputation with complicated missing patterns," *Transportation research part C: emerging technologies*, vol. 119, p. 102730, 2020.
- [8] Y. Ye, S. Zhang, and J. J. Yu, "Spatial-temporal traffic data imputation via graph attention convolutional network," in *International Conference on Artificial Neural Networks*. Springer, 2021, pp. 241–252.
- [9] T. Nie, G. Qin, and J. Sun, "Truncated tensor Schatten p-norm based approach for spatiotemporal traffic data imputation with complicated missing patterns," *Transportation research part C: emerging technologies*, vol. 141, p. 103737, 2022.
- [10] T. Nie, G. Qin, Y. Wang, and J. Sun, "Correlating sparse sensing for large-scale traffic speed estimation: A laplacian-enhanced low-rank tensor kriging approach," *Transportation Research Part C: Emerging Technologies*, vol. 152, p. 104190, 2023.
- [11] X. Wang, Y. Wu, D. Zhuang, and L. Sun, "Low-rank hankel tensor completion for traffic speed estimation," *IEEE Transactions on Intelligent Transportation Systems*, vol. 24, no. 5, pp. 4862–4871, 2023.
- [12] X. Chen, M. Lei, N. Saunier, and L. Sun, "Low-rank autoregressive tensor completion for spatiotemporal traffic data imputation," *IEEE Transactions on Intelligent Transportation Systems*, vol. 23, no. 8, pp. 12 301–12 310, 2021.
- [13] S. Liu, X. Li, G. Cong, Y. Chen, and Y. Jiang, "Multivariate time-series imputation with disentangled temporal representations," in *The Eleventh International Conference on Learning Representations*, 2022.
- [14] W. Ma and G. H. Chen, "Missing not at random in matrix completion: The effectiveness of estimating missingness probabilities under a low nuclear norm assumption," *Advances in neural information processing systems*, vol. 32, 2019.
- [15] N. Muhammad, N. Bibi, A. Jahangir, and Z. Mahmood, "Image denoising with norm weighted fusion estimators," *Pattern Analysis and Applications*, vol. 21, pp. 1013–1022, 2018.
- [16] W. Cao, D. Wang, J. Li, H. Zhou, L. Li, and Y. Li, "Brits: Bidirectional recurrent imputation for time series," *Advances in neural information processing systems*, vol. 31, 2018.
- [17] Z. Che, S. Purushotham, K. Cho, D. Sontag, and Y. Liu, "Recurrent neural networks for multivariate time series with missing values," *Scientific reports*, vol. 8, no. 1, p. 6085, 2018.
- [18] A. Cini, I. Marisca, and C. Alippi, "Filling the gaps: Multivariate time series imputation by graph neural networks," *arXiv preprint arXiv:2108.00298*, 2021.
- [19] W. Du, D. Côté, and Y. Liu, "Saits: Self-attention-based imputation for time series," *Expert Systems with Applications*, vol. 219, p. 119619, 2023.
- [20] I. Marisca, A. Cini, and C. Alippi, "Learning to reconstruct missing data from spatiotemporal graphs with sparse observations," *Advances in Neural Information Processing Systems*, vol. 35, pp. 32 069–32 082, 2022.
- [21] M. Liu, H. Huang, H. Feng, L. Sun, B. Du, and Y. Fu, "Pristi: A conditional diffusion framework for spatiotemporal imputation," *arXiv preprint arXiv:2302.09746*, 2023.
- [22] J. Ma, Z. Shou, A. Zareian, H. Mansour, A. Vetro, and S.-F. Chang, "Cds: cross-dimensional self-attention for multivariate, geo-tagged time series imputation," *arXiv preprint arXiv:1905.09904*, 2019.

- [23] A. Das, W. Kong, R. Sen, and Y. Zhou, "A decoder-only foundation model for time-series forecasting," *arXiv preprint arXiv:2310.10688*, 2023.
- [24] A. Garza and M. Mergenthaler-Canseco, "Timegpt-1," *arXiv preprint arXiv:2310.03589*, 2023.
- [25] P. Sharma, J. T. Ash, and D. Misra, "The truth is in there: Improving reasoning in language models with layer-selective rank reduction," *arXiv preprint arXiv:2312.13558*, 2023.
- [26] S. Van Buuren and K. Groothuis-Oudshoorn, "mice: Multivariate imputation by chained equations in r," *Journal of statistical software*, vol. 45, pp. 1–67, 2011.
- [27] X. Yi, Y. Zheng, J. Zhang, and T. Li, "St-mvl: filling missing values in geo-sensory time series data," in *Proceedings of the 25th International Joint Conference on Artificial Intelligence*, 2016.
- [28] H.-F. Yu, N. Rao, and I. S. Dhillon, "Temporal regularized matrix factorization for high-dimensional time series prediction," *Advances in neural information processing systems*, vol. 29, 2016.
- [29] X. Chen and L. Sun, "Bayesian temporal factorization for multidimensional time series prediction," *IEEE Transactions on Pattern Analysis and Machine Intelligence*, vol. 44, no. 9, pp. 4659–4673, 2021.
- [30] M. Jin, H. Y. Koh, Q. Wen, D. Zambon, C. Alippi, G. I. Webb, I. King, and S. Pan, "A survey on graph neural networks for time series: Forecasting, classification, imputation, and anomaly detection," *arXiv preprint arXiv:2307.03759*, 2023.
- [31] Y. Luo, X. Cai, Y. Zhang, J. Xu et al., "Multivariate time series imputation with generative adversarial networks," *Advances in neural information processing systems*, vol. 31, 2018.
- [32] J. Yoon, J. Jordon, and M. Schaar, "Gain: Missing data imputation using generative adversarial nets," in *International conference on machine learning*. PMLR, 2018, pp. 5689–5698.
- [33] Y. Luo, Y. Zhang, X. Cai, and X. Yuan, "E2gan: End-to-end generative adversarial network for multivariate time series imputation," in *Proceedings of the 28th international joint conference on artificial intelligence*. AAAI Press Palo Alto, CA, USA, 2019, pp. 3094–3100.
- [34] Y. Liu, R. Yu, S. Zheng, E. Zhan, and Y. Yue, "Naomi: Non-autoregressive multiresolution sequence imputation," *Advances in neural information processing systems*, vol. 32, 2019.
- [35] Y. Tashiro, J. Song, Y. Song, and S. Ermon, "Csdi: Conditional score-based diffusion models for probabilistic time series imputation," *Advances in Neural Information Processing Systems*, vol. 34, pp. 24 804–24 816, 2021.
- [36] S. Shan, Y. Li, and J. B. Oliva, "Nrtsi: Non-recurrent time series imputation," in *ICASSP 2023-2023 IEEE International Conference on Acoustics, Speech and Signal Processing (ICASSP)*. IEEE, 2023, pp. 1–5.
- [37] Y. Liang, Z. Zhao, and L. Sun, "Memory-augmented dynamic graph convolution networks for traffic data imputation with diverse missing patterns," *Transportation Research Part C: Emerging Technologies*, vol. 143, p. 103826, 2022.
- [38] Y. Wu, D. Zhuang, A. Labbe, and L. Sun, "Inductive graph neural networks for spatiotemporal kriging," in *Proceedings of the AAAI Conference on Artificial Intelligence*, vol. 35, no. 5, 2021, pp. 4478–4485.
- [39] W. Liang, Y. Li, K. Xie, D. Zhang, K.-C. Li, A. Souri, and K. Li, "Spatial-temporal aware inductive graph neural network for c-its data recovery," *IEEE Transactions on Intelligent Transportation Systems*, 2022.
- [40] T. Nie, G. Qin, Y. Wang, and J. Sun, "Towards better traffic volume estimation: Jointly addressing the underdetermination and nonequilibrium problems with correlation-adaptive gnns," *Transportation Research Part C: Emerging Technologies*, vol. 157, p. 104402, 2023.
- [41] A. Vaswani, N. Shazeer, N. Parmar, J. Uszkoreit, L. Jones, A. N. Gomez, L. Kaiser, and I. Polosukhin, "Attention is all you need," in *Advances in Neural Information Processing Systems*, 2017, pp. 5998–6008.
- [42] J. Dong, H. Wu, H. Zhang, L. Zhang, J. Wang, and M. Long, "Simmtm: A simple pre-training framework for masked time-series modeling," *arXiv preprint arXiv:2302.00861*, 2023.
- [43] Y. Nie, N. H. Nguyen, P. Sinthong, and J. Kalagnanam, "A time series is worth 64 words: Long-term forecasting with transformers," *arXiv preprint arXiv:2211.14730*, 2022.
- [44] Z. Li, Z. Rao, L. Pan, P. Wang, and Z. Xu, "Ti-mae: Self-supervised masked time series autoencoders," *arXiv preprint arXiv:2301.08871*, 2023.
- [45] J. Gao and B. Ribeiro, "On the equivalence between temporal and static equivariant graph representations," in *International Conference on Machine Learning*. PMLR, 2022, pp. 7052–7076.
- [46] G. Liu, "Time series forecasting via learning convolutionally low-rank models," *IEEE Transactions on Information Theory*, vol. 68, no. 5, pp. 3362–3380, 2022.
- [47] Z. Shao, Z. Zhang, F. Wang, W. Wei, and Y. Xu, "Spatial-temporal identity: A simple yet effective baseline for multivariate time series forecasting," in *Proceedings of the 31st ACM International Conference on Information & Knowledge Management*, 2022, pp. 4454–4458.
- [48] T. Nie, G. Qin, Y. Wang, and J. Sun, "Nexus sine qua non: Essentially connected neural networks for spatial-temporal forecasting of multivariate time series," *arXiv preprint arXiv:2307.01482*, 2023.
- [49] A. Zeng, M. Chen, L. Zhang, and Q. Xu, "Are transformers effective for time series forecasting?" *arXiv preprint arXiv:2205.13504*, 2022.
- [50] Z. Wu, S. Pan, G. Long, J. Jiang, X. Chang, and C. Zhang, "Connecting the dots: Multivariate time series forecasting with graph neural networks," in *Proceedings of the 26th ACM SIGKDD International Conference on Knowledge Discovery and Data Mining*. New York, NY, USA: Association for Computing Machinery, 2020, p. 753–763.
- [51] A. Cini, I. Marisca, D. Zambon, and C. Alippi, "Taming local effects in graph-based spatiotemporal forecasting," *arXiv preprint arXiv:2302.04071*, 2023.
- [52] H. Liu, Z. Dong, R. Jiang, J. Deng, J. Deng, Q. Chen, and X. Song, "Spatio-temporal adaptive embedding makes vanilla transformer sota for traffic forecasting," in *Proceedings of the 32nd ACM International Conference on Information and Knowledge Management*, 2023, pp. 4125–4129.
- [53] Y. Zhang and J. Yan, "Crossformer: Transformer utilizing cross-dimension dependency for multivariate time series forecasting," in *The Eleventh International Conference on Learning Representations*, 2022.
- [54] S. Wang, B. Z. Li, M. Khabsa, H. Fang, and H. Ma, "Linformer: Self-attention with linear complexity," *arXiv preprint arXiv:2006.04768*, 2020.
- [55] J. Liu, P. Musialski, P. Wonka, and J. Ye, "Tensor completion for estimating missing values in visual data," *IEEE transactions on pattern analysis and machine intelligence*, vol. 35, no. 1, pp. 208–220, 2012.
- [56] T. G. Kolda and B. W. Bader, "Tensor decompositions and applications," *SIAM review*, vol. 51, no. 3, pp. 455–500, 2009.
- [57] Z. Wu, S. Pan, G. Long, J. Jiang, and C. Zhang, "Graph wavenet for deep spatial-temporal graph modeling," *arXiv preprint arXiv:1906.00121*, 2019.
- [58] Z. Shao, Z. Zhang, F. Wang, and Y. Xu, "Pre-training enhanced spatial-temporal graph neural network for multivariate time series forecasting," in *Proceedings of the 28th ACM SIGKDD Conference on Knowledge Discovery and Data Mining*, 2022, pp. 1567–1577.
- [59] Z. Shen, M. Zhang, H. Zhao, S. Yi, and H. Li, "Efficient attention: Attention with linear complexities," in *Proceedings of the IEEE/CVF winter conference on applications of computer vision*, 2021, pp. 3531–3539.
- [60] S. Bhojanapalli, C. Yun, A. S. Rawat, S. Reddi, and S. Kumar, "Low-rank bottleneck in multi-head attention models," in *International conference on machine learning*. PMLR, 2020, pp. 864–873.
- [61] G. H. Golub and C. F. Van Loan, *Matrix computations*. JHU press, 2013.
- [62] G. Liu and W. Zhang, "Recovery of future data via convolution nuclear norm minimization," *IEEE Transactions on Information Theory*, vol. 69, no. 1, pp. 650–665, 2022.
- [63] X. Chen, Z. Cheng, N. Saunier, and L. Sun, "Laplacian convolutional representation for traffic time series imputation," *arXiv preprint arXiv:2212.01529*, 2022.
- [64] H. Wu, T. Hu, Y. Liu, H. Zhou, J. Wang, and M. Long, "Timesnet: Temporal 2d-variation modeling for general time series analysis," *arXiv preprint arXiv:2210.02186*, 2022.
- [65] C. Chen, K. Petty, A. Skabardonis, P. Varaiya, and Z. Jia, "Freeway performance measurement system: mining loop detector data," *Transportation Research Record*, vol. 1748, no. 1, pp. 96–102, 2001.
- [66] C. for Energy Regulation (CER), "CER Smart Metering Project - Electricity Customer Behaviour Trial, 2009-2010," [dataset] 1st Edition. Irish Social Science Data Archive. SN: 0012-00. <https://www.ucd.ie/issda/data/commissionforenergyregulationcer/>, 2012.
- [67] Y. Li, R. Yu, C. Shahabi, and Y. Liu, "Diffusion convolutional recurrent neural network: Data-driven traffic forecasting," *arXiv preprint arXiv:1707.01926*, 2017.

- [68] X. Zhang, Z. Zhao, T. Tsiligkaridis, and M. Zitnik, “Self-supervised contrastive pre-training for time series via time-frequency consistency,” *Advances in Neural Information Processing Systems*, vol. 35, pp. 3988–4003, 2022.